



Deep Learning for Computational Cytology: A Survey

Hao Jiang^a, Yanning Zhou^b, Yi Lin^a, Ronald CK Chan^c, Jiang Liu^d, Hao Chen^{a,*}

^aDepartment of Computer Science and Engineering, The Hong Kong University of Science and Technology, Hong Kong, China

^bDepartment of Computer Science and Engineering, The Chinese University of Hong Kong, Hong Kong, China

^cDepartment of Anatomical and Cellular Pathology, The Chinese University of Hong Kong, Hong Kong, China

^dSchool of Computer Science and Engineering, Southern University of Science and Technology, Shenzhen, China

ARTICLE INFO

Article history:

Received XX

Received in final form XX

Accepted XX

Available online XX

Keywords: Artificial Intelligence, Deep Learning, Computational Cytology, Pathology, Cancer Screening, Survey

ABSTRACT

Computational cytology is a critical, rapid-developing, yet challenging topic in the field of medical image computing which analyzes the digitized cytology image by computer-aided technologies for cancer screening. Recently, an increasing number of deep learning (DL) algorithms have made significant progress in medical image analysis, leading to the boosting publications of cytological studies. To investigate the advanced methods and comprehensive applications, we survey more than 120 publications of DL-based cytology image analysis in this article. We first introduce various deep learning methods, including fully supervised, weakly supervised, unsupervised, and transfer learning. Then, we systematically summarize the public datasets, evaluation metrics, versatile cytology image analysis applications including classification, detection, segmentation, and other related tasks. Finally, we discuss current challenges and potential research directions of computational cytology.

© 2022 Elsevier B. V. All rights reserved.

1. Introduction

Cytology is a branch of pathology to study the cells under microscopes to analyze the cellular morphology, and compositions, usually for cancer screening (Davey et al., 2006; Alberts et al., 2015; O'Flynn et al., 2021). Compared with histopathology, cytology focuses on the pathological characteristics of cells instead of tissues, which is a collection of thousands of cells in a specific architecture (Morrison and DeNicola, 1993; Dey, 2018). Cells being the structural and functional unit of living organisms (Alberts et al., 2003), their morphologies reflect the biological of the organ and even the body (Johnston, 1952; Skaarland, 1986; Ji et al., 2020). The clinical cytology testing procedure can be divided into collection and preservation, centrifugation, slide making, and staining (Fig. 1(A)). For

cytology screening, cytologists observe cytology slides under microscopes and analyze the properties and morphologies of cells (Fig. 1(B)). These slides can be also scanned into whole slide images (WSI) (Fig. 1(C)) for further digital analysis and processing. In addition, there are three types of cytology specimens, depending on the collection techniques: 1) Exfoliative cytology, including sputum, urine sediment, pleural effusion, and ascites (Maharjan et al., 2017). 2) Abrasive cytology, including cervical scraping, gastrointestinal tract, and endoscopic brushing (Kour Raina et al., 2021). 3) Aspiration cytology, also named fine-needle aspiration cell inspection (FNAC) (Lever et al., 1985) usually from breast, thyroid, and lung (Koss and Melamed, 2006; Ivanovic, 2014). Unlike histology, cytology specimens do not require removal of intact sizable tissue, allowing much less invasive sampling procedures. Therefore, the sampling is frequently painless, low-cost, and equipment-undemanding, making cytology useful for cancer screening and early diagnosis (Kitchener et al., 2006).

*Corresponding author.

E-mail address: jhc@cse.ust.hk (Dr. Hao Chen).

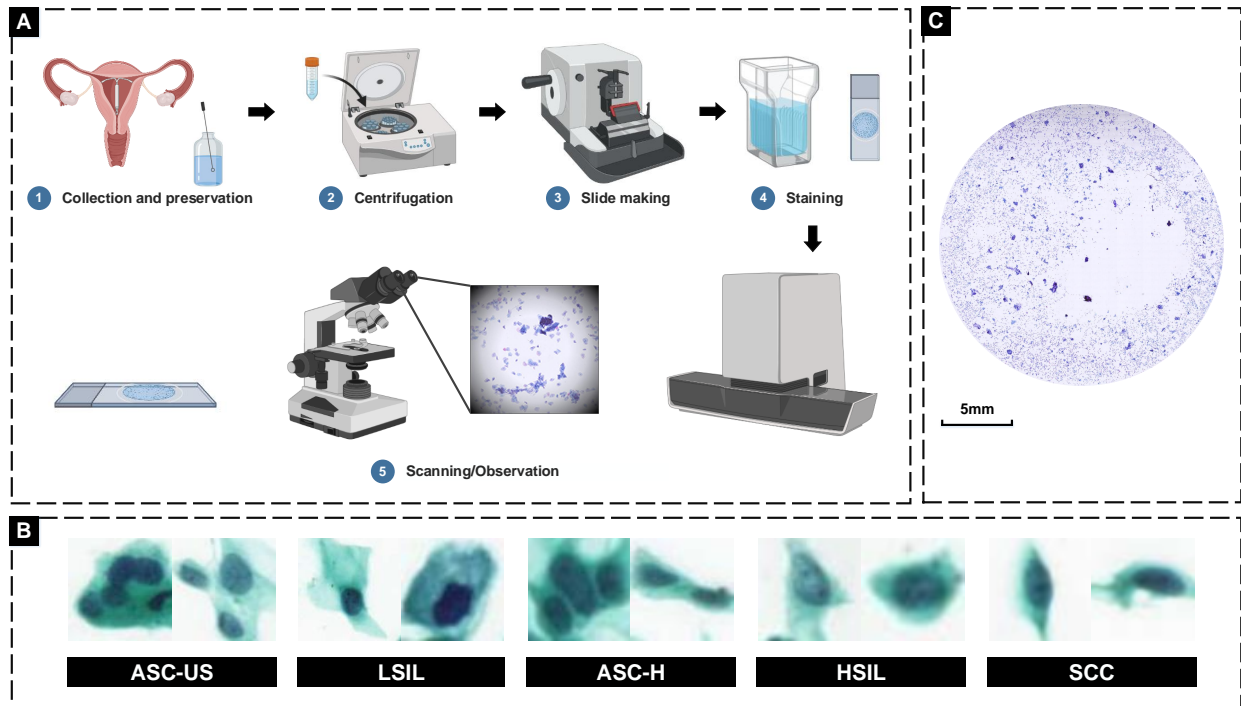


Fig. 1: Illustration of clinical cytology screening. (A) The procedure of cytology specimen preparation (taking the cervix as an example). (B) Cytology images in different categories. (C) WSI for digital analysis and processing.

Diagnosing cytological specimens is a highly professional task, requiring formal training and assessments overseen by international bodies. Currently, there is a trend to standardize cytological diagnosis reporting, allowing reports and implied risk of cancers to be understood by clinicians without ambiguity (Barkan *et al.*, 2016). It also provides well-defined features to be looked for among the cells being examined. Fig. 2 illustrates typical cytological morphologies of commonly encountered specimens. Specifically, cytology screening was first applied in cervix cancers almost 100 years ago. Present reporting of cervical cytology is guided by the Bethesda system (Nayar and Wilbur, 2015). Pre-cancerous and cancerous cells are first categorized into squamous cells and glandular cells, then they can be identified and graded by combinations of cytological features including enlarged nuclei, multinucleation, perinuclear halo, increased nuclear to cytoplasm ratio, wrinkled nuclear membrane, dyskeratosis (abnormal keratin formation), prominent nucleoli and tumor diathesis. Following the success of Bethesda system, present reporting of breast aspiration cytology is guided by Field *et al.* (2019). Aspiration of malignant breast lesions are often hypercellular and the cancer cells possess large sometimes irregular nuclei with prominent nucleoli and the lack of myoepithelial cells. Different grades of atypia were also established to estimate the risk of malignancy (Beca and Schmitt, 2019). Similarly, bladder cancer cells from urine often show irregular nuclei with very high N/C ratio (>0.7), prominent nucleoli and clumped/coarse chromatin, as outlined in Rosenthal *et al.* (2016). Thyroid cancer aspirates show distinctive features including papillary structures, psammoma bodies and optically clear nuclei with nuclear grooves and nuclear

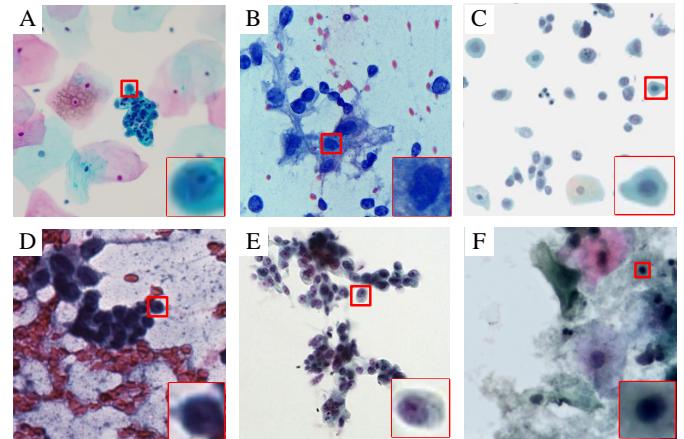


Fig. 2: Typical cytological morphologies of commonly encountered specimens, including (A) Cervix (Zhou *et al.*, 2019a), (B) Breast (Saikia *et al.*, 2019), (C) Urine (Awan *et al.*, 2021), (D) Thyroid (Dov *et al.*, 2021), (E) Lung (Teramoto *et al.*, 2017), (F) Oral (Matias *et al.*, 2021). Single cellular structures are zoomed by red boxes.

inclusions (Cibas and Ali, 2017). Together with examples from lung and oral mucosa illustrated in Fig. 2, cytological morphology from different organs provides diagnostic information for cancer screening and guide patient management at a minimal cost (Caddy *et al.*, 2005; Kontzoglou *et al.*, 2005).

In clinical cytology screening, scrutinizing every cell under the microscope (or in gigapixel whole slide images) in search of malignancy can be very time-consuming and tedious for cytologists (Mehrotra *et al.*, 2011; De Vito *et al.*, 2014). Con-

sidering ever increase in caseload, researchers have attempted to develop automatic methods for accurate and efficient cancer screening. The first successful trial could date back to the 1950s when an automatic screening system was developed for cervix (Tolles and Bostrom, 1956; Tolles, 1955). Afterwards, a series of cervical screening systems were launched with varying market success (Koss *et al.*, 1994; Wilbur *et al.*, 2009; Brown and Garber, 1999). These automated cytology screening systems have been shown to improve the efficiency without compromising accuracy of cytology screening procedures.

In recent decades, the automation technology and artificial intelligence (AI) have achieved remarkable progress in the field of medicine. Machine learning (ML), which is a subfield of AI, focuses on learning algorithms to represent the underlying patterns of data by imitating human beings. With rapid progress in ML, medical image interpretation and computer assisted-diagnosis in pathology (e.g., histopathology, cytology (Chen *et al.*, 2016a; Zhao *et al.*, 2019; Zhu *et al.*, 2021)), and radiology (e.g., computed tomography (CT), magnetic resonance imaging (MRI), X-ray, ultrasound (Lassau *et al.*, 2021; Jónsson *et al.*, 2019; Çalli *et al.*, 2021)). For cytology, previous studies demonstrated the feasibility of various ML approaches in cytology image analysis, including support vector machine (SVM), fuzzy c-means (FCM) (Chankong *et al.*, 2014), k-means (Isa (2005), and fuzzy clustering (Plissiti *et al.*, 2009). However, there remains challenges in these machine learning algorithms, such as developing accurate and efficient cytology image analysis approaches, establishing human-machine collaborative cytological screening systems.

Deep learning, as a branch of the ML family, was developed with multilayers neural networks for leveraging feature representations of input data. DL aims to reduce the heavy reliance on task-related features designed from expert knowledge in traditional ML approaches. It can also increase the model's capability of feature representation by end-to-end learning. In computational cytology, DL could provide cytologists with feasible solutions for accurate and efficient cytological screening. These approaches have been widely investigated in versatile types of cancers, such as cervix (Rahaman *et al.*, 2020), breast (Garud *et al.*, 2017), bladder (Dov *et al.*, 2021), and lung (Teramoto *et al.*, 2017). Among these DL-based methods, supervised learning involves mapping input images to predefined labels and it has been the most commonly developed DL scheme. Most existing studies on cytological applications focus on improving DL models performance by introducing specific constraints or architecture designs of DL models, such as introducing morphological constraints (Zhou *et al.*, 2019b; Chai *et al.*, 2021; Chen *et al.*, 2017).

The advancement of DL has greatly accelerated the development of computational cytology. There is a 10-fold increase in DL-based computational research from 2014 to 2021 with a booming trend in recent two years. The number of related publications is illustrated in Fig. 3, after searching literature databases (Google Scholar, PubMed, and arXiv). These publications focus on developing various DL approaches for cytological screening, such as classifying between normal and abnormal cells (Zhang *et al.*, 2017), locating and identifying cells

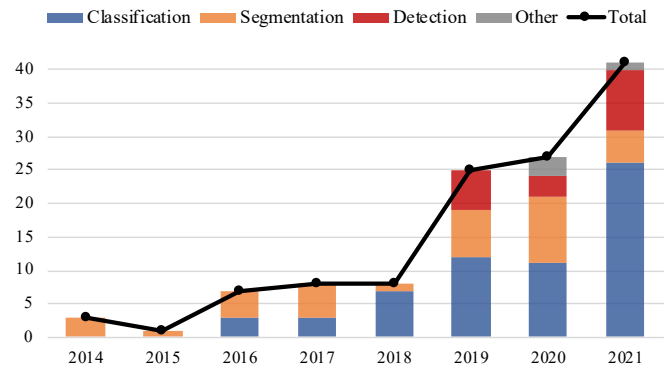


Fig. 3: Number of publications in deep learning-based computational cytology of classification, detection, segmentation and other tasks.

in cytological smears (Pirovano *et al.*, 2021), and segmentation of different cellular compartments (Zhou *et al.*, 2020).

There exists several surveys in the field of cytology image analysis (Landau and Pantanowitz, 2019; Mitra *et al.*, 2021; Rahaman *et al.*, 2020). However, these reviews were far from exhaustive in terms of the advanced algorithms, publicly available datasets, and promising trends in this field. Besides, most of the DL-based cytology surveys focused on the cervix, ignoring the progress in other types of cancer, such as lung and bladder (Rahaman *et al.*, 2020). Afterwards, Mitra *et al.* (2021) focused on various cytology applications instead of analyzing them in the DL methodology perspective. In this paper, we have surveyed over 120 publications since 2014, and systematically reviewed the progress of DL approaches and techniques in computational cytology, also covering cytology specimens from various parts of the body.

There are six sections in this paper. **Section 1** briefly introduces the background and objective of this review. **Section 2** gives an overview of different learning approaches in the context of computational cytology. **Section 3** summarizes public cytology datasets and common evaluation metrics. **Section 4** presents the progress and achievements on the DL-based cytology image analysis. **Section 5** discusses existing challenges and potential research directions in computational cytology. **Section 6** concludes this survey paper.

2. Deep learning methodology

In this section, we present the definition, formulations, and general procedures of DL methods, which can be developed for various cytological applications. According to the availability of annotations, DL can be categorized as supervised learning (section 2.1), weakly supervised learning (section 2.2), unsupervised learning (section 2.3), together with transfer learning (section 2.4).

2.1. Supervised learning

Supervised learning aims to learn functional mappings between input data and corresponding labels. For medical image

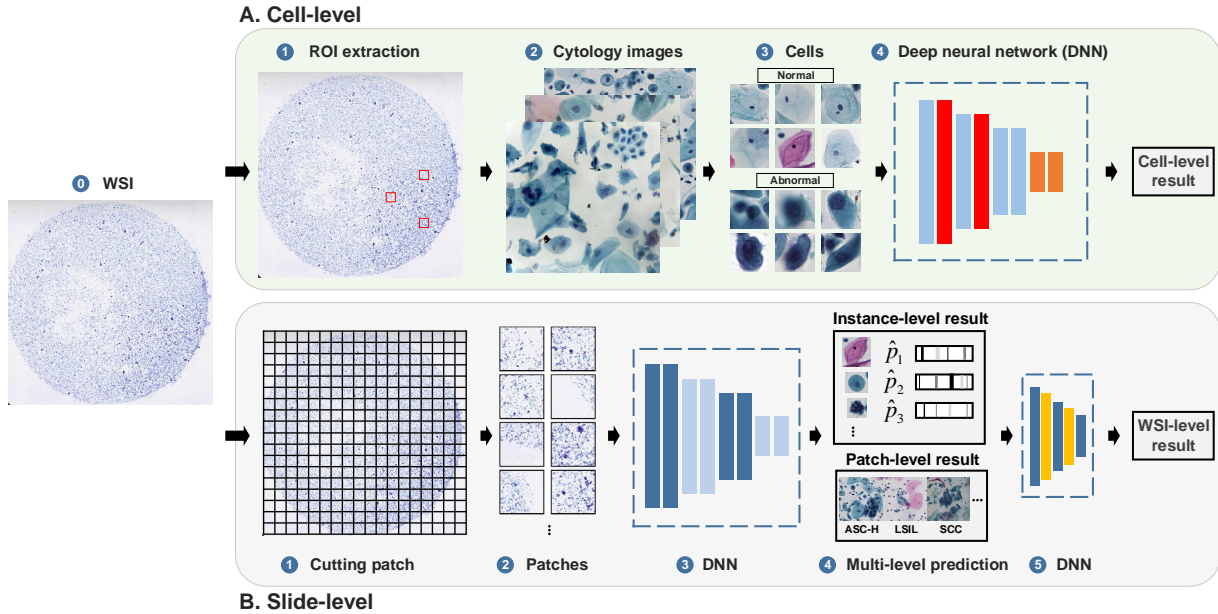


Fig. 4: Standard workflow of DL-based supervised learning for cytological classification. (A) Cell-level: Firstly, ROIs are extracted from WSIs and cut into cell patches, then they are input into the DNN for extracting features and predicting category of each cell patch. (B) Slide-level: Patches cut from WSIs are input into a DNN to obtain multi-level predictions (e.g., instance-level and patch-level), then these predictions are used to predict final WSI-level results.

analysis, the inputs are medical images, while labels are varied according to different tasks, e.g., image-level categories for classification, object-level localizations (e.g., boxes, points) for detection, and pixel-wise masks for segmentation. Formally, the input images $X = \{x_i\}_{i=1}^N$ together with corresponding labels $Y = \{y_i\}_{i=1}^N$ are used to train a predictive model by minimizing the objective function. The typical deep models in supervised learning include multilayer perceptron (MLP) (Rosenblatt, 1961), convolutional neural network (CNN) (LeCun et al., 1998), recurrent neural network (RNN) (Zaremba et al., 2014), and transformer (Tay et al., 2020).

CNN is regarded as the most successful DL architecture in image analysis (Litjens et al., 2017). It mainly consists of three types of hidden layers: convolutional layers for feature extraction, pooling layers for reducing the feature resolution, and fully connected layers for compiling the features extracted by previous layers and outputting prediction results. Then, backpropagation algorithm is introduced to update parameters of different layers during training (LeCun et al., 1998). Due to the strategies of local receptive fields, shared weights, and downsampling in pooling layers, CNN has achieved great success in many image analysis tasks, such as autonomous driving (Rosenzweig and Bartl, 2015), face recognition (Wang and Deng, 2021), and biomedicine (Litjens et al., 2017).

Commonly-used CNN architectures in computer vision fields have been employed and developed for various cytological applications, e.g., AlexNet (Mohammed et al., 2021), VGGNet (Albuquerque et al., 2021), ResNet (Miselis et al., 2019). Currently, most cytology researches focus on developing new algorithms based on these basic architectures in various DL tasks: classification, detection, and segmentation (Lin et al., 2019b; Sornapudi et al., 2019; Hussain et al., 2020c).

Classification. This classification model aims at predicting the category of the input image. It can be essentially formulated as $\hat{y} = f(x, \theta)$, where x and \hat{y} is input image and its predicted category, and θ represents learnable parameters of classification architecture. For training these architectures, cross-entropy loss L_{CE} measures the discrepancy between predicted probability \hat{y}_{ic} and true label y_{ic} by probability distribution:

$$L_{CE} = -\frac{1}{N} \sum_{i=1}^N \sum_{c=1}^M y_{ic} \log(\hat{y}_{ic}) \quad (1)$$

where, N is the amount of image samples, and M is the number of categories. Then, the prediction loss is used to optimize parameters θ of network by backpropagation (Rumelhart et al., 1986).

Usually, the label space of the cytology image refers to its benign/malignant or sub-category. In the standard cell-level classification workflow, regions of interest (ROIs) are extracted from collected slides by cytologists or technicians. Then, ROIs are cut into cell patches as input of deep models. After that, a DL-based feature extractor is responsible for representing high-level features and outputting prediction categories (Fig. 4). For slide-level screening, existing studies mainly divide this task into two stages: First, the deep neural network (e.g., CNN, RNN, and Transformer) is responsible for predicting multi-level results, such as detection of malignant or benign cells and the category of patches. Then, another network aggregates these results and predicts the final WSI-level results (Wei et al., 2021; Lin et al., 2021).

Detection. Unlike classification, the detection task is to locate objects from whole images and predict categories of these objects. Thus, it can be regarded as the combination of two

tasks: regressing the object's location and classifying the types of objects. CNN-based object detection algorithms are mainly divided into two categories: two-stage method and one-stage method. In two-stage, the workflow includes feature extraction, region proposal, and prediction. The first stage is to regress coarse prediction (box location and predicted probability) by region proposal. The second stage aims to output fine predictions (box location and object category). Typical models for two-stage algorithms include R-CNN (Girshick *et al.*, 2014), Fast R-CNN (Girshick, 2015), Faster R-CNN (Ren *et al.*, 2015). One-stage detection methods aim to abandon the strategy of region proposal. Instead, they directly predict the category and location of the objects in an end-to-end architecture, including SSD (Liu *et al.*, 2016), YOLO (Redmon *et al.*, 2016), FCOS (Tian *et al.*, 2019) and RetinaNet Lin *et al.* (2017b).

There are two types of loss functions in object detection task, classification loss and location loss. For classification loss, by improving L_{CE} , focal loss L_{focal} is proposed in RetinaNet to balance classification samples (Lin *et al.*, 2017b):

$$L_{focal} = \begin{cases} -\alpha(1-p)^\gamma \log(p), & \text{if } y = 1 \\ -(1-\alpha)p^\gamma \log(1-p), & \text{if } y = 0 \end{cases} \quad (2)$$

where p is the model's estimated probability with label y , and γ and α are tunable parameters. For location loss, mean absolute error loss L_{MAE} calculates the average distance between the predicted and the true locations:

$$L_{MAE} = \frac{\sum_{i=1}^N |f(x_i) - y_i|}{N} \quad (3)$$

Then, intersection over union (IoU) loss was introduced to calculate the loss of predicted boxes instead of coordinates in L_{MAE} (Yu *et al.*, 2016):

$$L_{IoU} = -\ln \frac{\text{Intersection}(box_{gt}, box_p)}{\text{Union}(box_{gt}, box_p)} \quad (4)$$

where box_{gt} and box_p represent ground truth box and predicted box, respectively. After that, some advanced loss functions are designed recently, including GIoU loss for non-intersection area (Rezatofighi *et al.*, 2019), CIoU loss for closing center points (Zheng *et al.*, 2020), etc.

In addition, there are still someFor example, fully common issues for both one-stage and two-stage algorithms. For example, multiple overlapping predicted boxes in the prediction results. These repetitive and redundant proposals can be removed by the strategy of non-maximum suppression (Neubeck and Van Gool, 2006).

Segmentation. This is a fundamental and essential task in medical image analysis. Segmentation is to make the pixel-wise prediction which represents the morphology of biomedical structures, such as cell (Zhou *et al.*, 2020), gland (Chen *et al.*, 2016b), and organ (Rahaman *et al.*, 2020). According to whether to distinguish each instance object, DL-based segmentation models can be divided into two branches: semantic segmentation and instance segmentation. Semantic segmentation aims to predict the category of each pixel to obtain masks

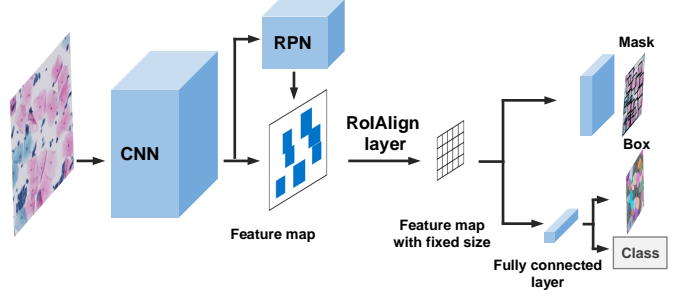


Fig. 5: Instance segmentation in cytology image analysis by Mask R-CNN.

of objects, which can be regarded as a pixel-wise classification task. Fully convolutional network (FCN) is one of the successful segmentation architectures, which replaced the fully connected layers in traditional CNN with convolutional layers for outputting segmentation map (Long *et al.*, 2015). Then, Falk *et al.* (2019) proposed U-Net for biomedical image segmentation by multi-scale feature fusion with a downsampling-upsampling architecture. In instance segmentation, models not only segment pixels into categories but also assigned them corresponding instance ID. Its popular structures mainly follow the detect-then-segment pipeline (Fig. 5). For instance, Mask R-CNN was proposed by introducing a mask prediction head based on Faster R-CNN (He *et al.*, 2017).

When training mentioned semantic and instance segmentation models, classification loss L_{CE} is introduced as the pixel-wise classification supervision for segmentation. Another widely-used loss function, dice coefficient loss L_{dice} is designed to measure the similarity between predicted masks Y_m and ground truth Y_{gt} by calculating the dice coefficient, and is defined as (Milletari *et al.*, 2016):

$$L_{dice} = 1 - \frac{2|Y_m \cap Y_{gt}|}{|Y_m| + |Y_{gt}|} \quad (5)$$

2.2. Weakly supervised learning

Weakly supervised learning is proposed for the scenarios where labels are not fully available, including incomplete supervision, inaccurate supervision, and inexact supervision (Zhou, 2018). Semi-supervised learning is one successful learning paradigm of incomplete supervision. It leverages both labeled and unlabeled data by extracting hidden information in unlabeled sets to enhance the feature representation of the labeled set. For inaccurate supervision, methods for noisy label problem can identify the potentially mislabeled samples and make corrections, thus improving the reliability of supervision.

Multi-instance learning (MIL) is an effective inexact supervision method, which aims at utilizing coarse-level annotations (e.g., image-level) for learning fine-level (e.g., pixel-level, patch-level) tasks (Maron and Lozano-Pérez, 1998; Xu *et al.*, 2014). The standard workflow of MIL is illustrated in Fig. 6. Firstly, a series of patches are extracted from whole images with patch-level annotations. Then, these patches are cut into instances and formed bags. Finally, a multi-instance classifier is established by learning for multi-instance bags, which is used for the prediction of unknown bags or instances.

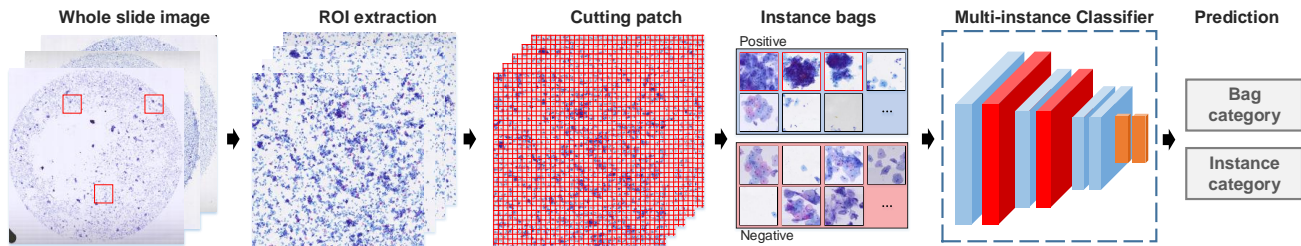


Fig. 6: Overview of multiple instance learning paradigm. Original WSIs are extracted to ROIs and cut into patches, then they are formed instance bags with bag-level label (positive or negative). For learning algorithms, these bags are used to learn a classification function that can predict the labels of bags and instances in the testing data.

Specifically, given a training dataset $\{(X_i, Y_i)_{i=1}^N\}$, where $X_i = \{x_{i1}, x_{i2}, \dots, x_{im}\}$ are instance bags, x_{im} is the m -th instance of the i -th bag. $Y_i \in \{-1, +1\}$ is its corresponding label of the i -th bag, $+1$ represents positive bag with at least one positive instance in this bag, and -1 represents negative bag with no positive instance. Then, bags X_i together with labels are used to learn a classification function that can predict the labels of bags and instances.

Weakly supervised learning is particularly appealing in computational cytology scenarios (e.g., whole slide thyroid malignancy prediction (Dov et al., 2021)), where full labels are expensive to obtain (Srinidhi et al., 2020). Because fully labeling of all lesions and cells in cytological screening WSIs is hardly possible for cytologists. Hence, weakly supervised learning is introduced to effectively represent and enhance features in the scenarios of limited annotations.

2.3. Unsupervised learning

Unsupervised learning is effective for learning useful and underlying representations from unlabeled data, which can be utilized for downstream tasks. For example, unsupervised image augmentation can increase the amount and variety of original dataset for increasing the performance of classification models. Afterwards, unsupervised stain transformation can be adopted to normalize datasets in preprocessing pathology images. Auto-encoder (AE) is a typical structure in unsupervised learning, which is formulated as: $P(x_i) \rightarrow z \rightarrow P(x'_i)$, where AE is trained to encode the input image x_i to obtain latent representation z . Then, decoders generate reconstructed image x'_i with the supervision of the raw input x_i .

Two typical unsupervised models have gained popularities: variational auto-encoder (VAE) (Larsen et al., 2016; Kingma and Welling, 2013) and generative adversarial network (GAN) (Goodfellow et al., 2014). As shown in Fig. 7(A), VAE improved AE by constraining latent variables to be normally distributed, then sampling a latent vector into a decoder for outputting the image. GAN is another promising architecture that can mitigate the difficulty of collecting large-scale labeled medical datasets by synthesizing high-quality fake images. For its structure, GAN is formed by a generator-discriminator architecture, as shown in Fig. 7(B). The generator aims to generate realistic images, while the discriminator competes with generator to differentiate real images and generated images. Therefore, this generator-discriminator architecture is optimized via

the adversarial training (Goodfellow et al., 2014):

$$\min_G \max_D V(D, G) = \mathbb{E}_{x \sim p_{\text{data}}(x)} [\log D(x)] + \mathbb{E}_{z \sim p_z(z)} [\log(1 - D(G(z)))] \quad (6)$$

where $G(\cdot)$ denotes the generator, and $D(\cdot)$ denotes the discriminator. $\mathbb{E}(\cdot)$ is the expectation value of distribution, $p_{\text{data}}(x)$ and $p_z(z)$ are the distribution of the real sample and noise, respectively. During training, generator $G(\cdot)$ aims to learn the distribution of real samples p_{data} , and discriminator $D(\cdot)$ is responsible for discriminating generated and real images, thus forcing the generator to generate realistic images. After the emergence of this basic GAN structure and adversarial loss, many advanced GAN models are proposed to satisfy higher requirements of generated images (e.g., quality, fidelity, and diversity) (Yi et al., 2019). For example, one promising architecture, CycleGAN is designed for style transformation between unpaired images (s, t), which is a symmetrical structure consisting of two generators $\{G_{S \rightarrow T}, G_{T \rightarrow S}\}$ for mutual generation between two domains (S and T), and two discriminators $\{D_S, D_T\}$ for discriminating generated images and images of respective domains. In addition, cycle consistency loss $L_{\text{cyc}}(G_{S \rightarrow T}, G_{T \rightarrow S})$ is designed for one-to-one mapping in CycleGAN architecture, defined as (Zhu et al., 2017):

$$L_{\text{cyc}}(G_{S \rightarrow T}, G_{T \rightarrow S}) = \mathbb{E}_{s \sim p_{\text{data}}(s)} [\|G_{T \rightarrow S}(G_{S \rightarrow T}(s)) - s\|_1] + \mathbb{E}_{t \sim p_{\text{data}}(t)} [\|G_{S \rightarrow T}(G_{T \rightarrow S}(t)) - t\|_1] \quad (7)$$

where $p_{\text{data}}(s)$ and $p_{\text{data}}(t)$ are the distribution of images in domain S and domain T .

In cytology, unsupervised learning algorithms have been designed for various DL tasks, such as stain conversion by CycleGAN (Teramoto et al., 2021), data augmentation for improving the accuracy of classification by cGAN (Dey et al., 2019), and generating high-resolution images by GAN-based super-resolution model (Ma et al., 2020).

2.4. Transfer Learning

Transfer learning is a subfield of deep learning that focuses on transferring knowledge from source to target domain for enhancing target tasks. Two transfer learning approaches are commonly used in medical image analysis, including fine-tuning and domain adaptation (DA).

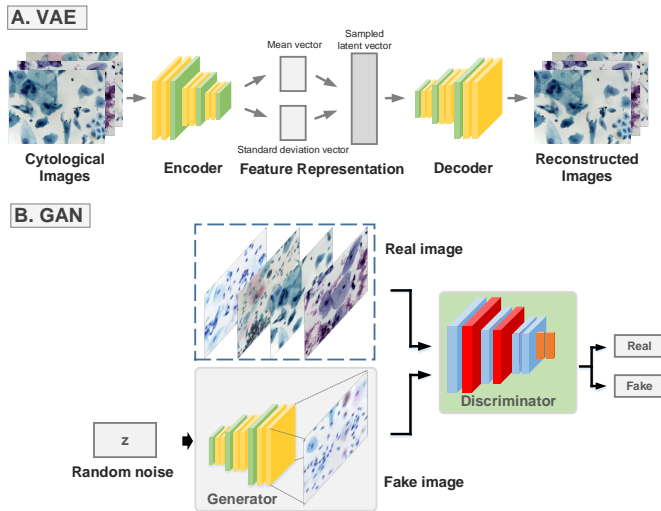


Fig. 7: AE-based unsupervised learning models. (A) Variational auto-encoder (VAE) improved AE by constraining the latent representation to be the normal distribution. (B) Generative adversarial network (GAN), which consists of a generator and a discriminator. The generator is responsible for generating fake images from random noise while discriminator forcing the generator generating realistic images by discriminating generated fake image and real image.

Fine-tuning is regarded as a common model initialization trick for training DL models. It can reduce the overfitting issue and improve the generalization capability of deep models by transferring knowledge from large public datasets (e.g., ImageNet (Deng *et al.*, 2009)) to domain-specific tasks (e.g., cervical cell classification) (Sornapudi *et al.*, 2019; Yosinski *et al.*, 2014). Formally, the goal of fine-tuning is training a task \mathcal{T}^t by a small dataset T . Specifically, it exploits a large-scale and task-similar \mathcal{T}^t dataset $S = \{s_i\}_{i=1}^M$ ($M \gg N$) to pre-train a network $f(\sim; \theta)$ first, then a small target dataset $T = \{t_i\}_{i=1}^N$ is used to train the several last layers of the pre-trained model for obtaining the target model N_t . Under the premise that different datasets for training similar tasks have similar low-level feature representations, fine-tuning is regarded as a common and effective training strategy in various DL tasks as well as cytology image analysis (Zhang *et al.*, 2017).

Domain adaptation (DA) is another transfer learning approach that transfers knowledge by learning to narrow the distribution gap of datasets in different domains. The paradigm of DA can be defined as: giving two different datasets (T and S) with different distributions ($p(S) \neq p(T)$), DA methods can align the distributions of these datasets by marginal, conditional or joint distribution adaptation. As a result, the knowledge is transferred from source to target domain, thus improving the performance of target models (Oza *et al.*, 2021). In medical image analysis, data heterogeneity hinders the successful practice of deep models in the clinic. This issue can be mitigated by domain adaptation for improving the validity and reproducibility of deep models clinically (Guan and Liu, 2021).

3. Datasets and metrics

Deep learning relies on large amounts of labeled data, we summarize publicly available datasets as well as representative

private datasets in cytology. As illustrated in Table 1, the majority of public datasets are from the cervix, with a small number of other cancer types, such as breast, oral, and stomach. These publicly available cytology datasets can be used to develop deep learning algorithms for various tasks, including classification, detection, and segmentation.

Herlev (Jantzen *et al.*, 2005). This database consists of 917 Papanicolaou (Pap) smear cervical images in 7 classes (3 normal cell classes and 4 abnormal cell classes), which are collected from the Herlev University Hospital. As the earliest established public cytology dataset, Herlev dataset is extensively adopted for developing DL-based coarse and fine-grained classification models for cervical cancer screening (Zhang *et al.*, 2017; Lin *et al.*, 2019b).

ISBI 2014 (Lu *et al.*, 2015). Another widely developed cervical dataset comes from the ISBI challenge. Different from Herlev dataset, this dataset focuses on the segmentation task with pixel-wise annotations. It consists of 16 non-overlapping fields of view images ($\times 40$ magnification) with 645 cells obtained from four cervical cytology specimens. Each sample in this dataset contains 20 to 60 Pap-stained cervical cells with varying degrees of overlapping.

ISBI 2015 (Lu *et al.*, 2016). ISBI 2015 extends ISBI 2014 dataset to 945 cervical cytology images by synthesizing. ISBI 2015 has a varying number of cells and different degrees of cell overlapping (size of 512×512 pixels), which contains 45 training images (taken from the 4 extended depth field images) and 900 testing images (from 12 images).

Sipakmed (Plissiti *et al.*, 2018). This database consists of 4049 images of isolated cells that have been manually cropped from 966 cluster cell images of Pap smear slides. Sipakmed dataset has 5 types of cervical cells, including superficial-intermediate, parabasal, koilocytotic, dyskeratotic, and metaplastic cells.

CERVIX93 (Phoulady and Mouton, 2018). This is the first dataset established for nuclei detection tasks in cytology. It consists of 93 stacks of images at $40\times$ magnification. Each stack has 10-20 images acquired at the equally spaced field of views from the top to the bottom of the slide. In this dataset, 2705 nuclei are annotated by bounding boxes with three different Pap test grades: negative, low-grade squamous in the intraepithelial lesion (LSIL) or high-grade squamous intraepithelial lesion (HSIL).

FNAC (Saikia *et al.*, 2019). This is the only public breast cytology dataset developed for classification model. These breast images are collected from 20 patients, comprising of 212 fine-needle aspiration cell inspection images in classes of benign (99) and malignant (113).

BHS (Araujo *et al.*, 2019). It collects 194 Pap-smear cervical slides from the Brazilian Health System (BHS). Among them, 108 images have at least one abnormal cell and 86 images with normal cells only. In sum, it has 5 types of abnormalities: carcinoma, HSIL, LSIL, atypical squamous cells of undetermined significance (ASC-US) and atypical squamous cells cannot exclude HSIL (ASC-H).

AgNOR (Amorim *et al.*, 2020). The dataset is composed of 2540 images with 1200×1600 pixels each. Different from

Table 1: Summary of publicly available and representative private databases in computational cytology

Reference/Year	Task	Organ	Stain	Size	Description	Link
Herlev 2005 (Jantzen <i>et al.</i> , 2005)	Classification	Cervix	Pap	variable	917 cells	http://mde-lab.aegean.gr/downloads
ISBI 2014 (Lu <i>et al.</i> , 2015)	Segmentation	Cervix	Pap	512 × 512	16 images (645 cells)	https://github.com/luzhi/cellsegmentation_TIP2015
ISBI 2015 (Lu <i>et al.</i> , 2016)	Segmentation	Cervix	Pap	512 × 512	945 images synthesized by ISBI 2014	http://goo.gl/KcpLrQ
Sipakmed 2018 (Plissiti <i>et al.</i> , 2018)	Classification	Cervix	Pap	2,048 × 1,536	966 images (4,049 annotated cells)	https://www.cs.uoi.gr/~marina/sipakmed.html
CERVIX93 2018 (Phoulady and Mouton, 2018)	Classification Detection	Cervix	Pap	1,280 × 960	93 stacks of images (2,705 nuclei)	https://github.com/parham-ap/cytology_dataset
FNAC 2019 (Saikia <i>et al.</i> , 2019)	Classification	Breast	Pap	2,048 × 1,536	212 images in two classes: benign (99) and malignant (113)	https://1drv.ms/u/s!A1-T6d-EMf6axsEbvhbEc2gUFs
BHS 2019 (Araujo <i>et al.</i> , 2019)	Segmentation Ranking	Cervix	Pap	1,392 × 1,040	194 images in classes of carcinoma, HSIL, LSIL, ASC-US and ASC-H	https://sites.google.com/view/centercric
AgNOR 2020 (Amorim <i>et al.</i> , 2020)	Segmentation	Cervix	AgNOR	1,600 × 1,200	2,540 images (4,515 nuclei)	https://arquivos.ufsc.br/d/373be2177a33426a9e6c/
LBC 2020 (Hussain <i>et al.</i> , 2020a)	Classification	Cervix	Pap	2,048 × 1,536	963 LBC images in classes of NILM, LSIL, HSIL, and SCC	https://data.mendeley.com/datasets/zddtpgzv63/4
Oral 2021 (Matias <i>et al.</i> , 2021)	Classification Detection Segmentation	Oral	Pap	1,200 × 1,600	1,934 images (4,287 annotations)	https://arquivos.ufsc.br/d/5035aec3c24f421a95d0/
Cric 2021 (Rezende <i>et al.</i> , 2021)	Classification	Cervix	Pap	1,376 × 1,020	400 images (11,534 cells)	https://database.cric.com.br
CDetector 2021 (Liang <i>et al.</i> , 2021b)	Detection	Cervix	Pap	224 × 224	7,410 images (48,587 object instance bounding boxes) in 11 classes	https://github.com/kuku-sichuan/ComparisonDetector
Ascites 2020 (Su <i>et al.</i> , 2020)	Classification Detection	Stomach	H&E, Pap	1,064 × 690	487 images for classification in two classes: malignant (18,558) and benign (6,089). 176 images for detection (6,573 annotated cell bounding boxes)	https://pan.baidu.com/s/1r0cd0Pvm5DiUmaNozMSxgg
RSDC 2021 (Ma <i>et al.</i> , 2021)	Super resolution	Cervix	Pap	128 × 128 (HR) 64 × 64 (LR)	5 slides (25000 patches)	https://www.kaggle.com/birkhoff007/rsdcdata
IRNet 2019 (Zhou <i>et al.</i> , 2019a)	Segmentation	Cervix	Pap	1,000 × 1,000	413 images (4,439 cytoplasm and 4,789 nuclei)	Private dataset
DCCL 2020 (Zhang <i>et al.</i> , 2019)	Detection	Cervix	Pap	1,200 × 2,000	1,167 WSIs (14,432 patches, and 27,972 labeled lesion cells)	Private dataset
Dual 2021 (Lin <i>et al.</i> , 2021)	Risk stratification	Cervix	Pap	Up to 50,000 × 50,000	19,303 WSIs in two classes: abnormal (202,557) and normal (272,933)	Private dataset
Hybrid 2021 (Zhu <i>et al.</i> , 2021)	Classification Detection Segmentation	Cervix	Pap	6000 × 6000	24 categories and 2000 images in each category, 81,727 smears (1.7 million annotated targets) for detection model	Private dataset

other public cervical datasets, it contains cells stained with the silver technique, which is known as argyrophilic nucleolar organizer regions (AgNOR). For developing segmentation approaches, experts annotate objects by the Labelme tool (Russell *et al.*, 2008), including nuclei, clusters, and satellites.

LBC (Hussain *et al.*, 2020a). Recently, liquid-based cytology (LBC) is developed for providing more uniform fixation with a cleaner background and well-preserved samples than con-

ventional Pap smear tests. This dataset consists of 963 images with four classes: NILM, LSIL, HSIL, and squamous cell carcinoma (SCC).

Oral (Matias *et al.*, 2021). Totally, 1,934 oral images of 1200 × 1600 pixels are acquired from two Pap-stained slides of cancer diagnosed oral brush samples. With different types of annotation (category, box, mask), various DL tasks can be conducted by this dataset, including classification, detection, and segmentation.

Table 2: Summary of evaluation metrics in computational cytology

Metric	Definition	Description	Application in cytology
Classification			
TP/TN/FP/FN	True Positive, True Negative, False Positive, False Negative	A test result that correctly indicates the presence of a condition (TP), correctly indicates the absence of a condition (TN), wrongly indicates the presence of a particular condition (FP), wrongly indicates the absence of a particular condition (FN).	Classification of FNAC images; formulate other metrics (e.g., accuracy, precision, recall) (Sanyal <i>et al.</i> , 2018; Liang <i>et al.</i> , 2021a).
Confusion matrix	A Matrix. Row: actual class; Column: predicted class.	The number of correct and incorrect predictions are summarized with count values and broken down by each class.	Classification of lung cancer sub-type; pap smear image; quantitative analysis of abnormalities; WSI-level risk stratification (Teramoto <i>et al.</i> , 2017; Mohammed <i>et al.</i> , 2021; Ke <i>et al.</i> , 2021; Awan <i>et al.</i> , 2021).
Accuracy (Acc)	$\frac{TP+TN}{FP+FN+TP+TN}$	Proportion of all positive and negative classes with correct predictions in all samples.	Cervical squamous lesions classification; FNAC image classification (Liu <i>et al.</i> , 2020; Bal <i>et al.</i> , 2021; Albuquerque <i>et al.</i> , 2021).
Precision (P)	$\frac{TP}{FP+TP}$	The proportion of positive samples classified as positive examples by the classifier.	Cervical cells classification; cervical lesions classification; multi-cell classification in liquid-based cytology images (Sornapudi <i>et al.</i> , 2019; Liu <i>et al.</i> , 2020; Rahaman <i>et al.</i> , 2021).
Recall (R)	$\frac{TP}{FN+TP}$	The proportion of the samples predicted to be positive cases in the total positive cases.	Pap smear image classification; classification of cervical cells (Mohammed <i>et al.</i> , 2021; Rahaman <i>et al.</i> , 2021).
Specificity (Spec)	$\frac{TN}{FP+TN}$	The proportion of samples that are correctly predicted as negative classes in all negative classes.	Cell classification; differential diagnosing of papillary thyroid carcinomas; detection of cervical intraepithelial neoplasia or invasive cancer (Zhang <i>et al.</i> , 2017; Guan <i>et al.</i> , 2019b; Bao <i>et al.</i> , 2020).
Sensitivity (Sens)	$\frac{TP}{FN+TP}$	The proportion of the samples predicted to be positive cases in the total positive cases.	Distinguish large cell neuroendocrine; identify cells; high resolution image classification (Gonzalez <i>et al.</i> , 2020; Li <i>et al.</i> , 2021).
F1-score (F1)	$\frac{2 \times \text{Precision} \times \text{Recall}}{\text{Precision} + \text{Recall}} = \frac{2 \times TP}{FP+FN+2TP}$	Harmonic average of precision and recall, and it is defined as the final evaluation index in many classification tasks.	Classification of cervical cells; multi-cell classification in liquid-based cytology images; cell image ranking (Sornapudi <i>et al.</i> , 2019; Araujo <i>et al.</i> , 2019; Rahaman <i>et al.</i> , 2021).
ROC curve	(FP rate, TP rate)	ROC is a graph showing the performance of a classification model at all classification thresholds.	Prediction of malignancy; cervical cancer screening; smear-level risk stratification (Elliott Range <i>et al.</i> , 2020; Tan <i>et al.</i> , 2021; Lin <i>et al.</i> , 2021).
AUC	Area under the ROC curve	The closer the AUC is to 1, the better the classifier performance.	Cancer screening (cell-level detection, patch-level and case-level classification); quantitative analysis of abnormalities; automating the paris system for cytopathology (Vaickus <i>et al.</i> , 2019; Ke <i>et al.</i> , 2021; Cao <i>et al.</i> , 2021).
Detection			
IoU	$\frac{P \cap GT}{P \cup GT} = \frac{TP}{FP+FN+TP}$	P denotes predicted bounding box, and GT is ground truth box. The ratio of the intersection and union of the predicted bounding box and the ground truth bounding box.	Nuclei/Cell detection; automation-assisted cervical cancer reading (Kilic <i>et al.</i> , 2019; Xiang <i>et al.</i> , 2020; Liang <i>et al.</i> , 2021a).
AP	Average precision	The mean value of precision on precision-recall curve.	Detection of abnormal cervical cells (Cao <i>et al.</i> , 2021).
mAP	mean AP	Average of AP in all categories.	Cell/Clumps detection; quantification of pulmonary hemosiderophages (Marzahl <i>et al.</i> , 2020; Chai <i>et al.</i> , 2021; Liang <i>et al.</i> , 2021b).
Segmentation			
Pixel Precision (P_p)	$\frac{TP_p}{TP_p+FP_p}$	The p means this is a pixel-level metric. Proportion of correctly segmented pixels to all segmented pixels.	Cytological examination (overlapping cell segmentation) (Tareef <i>et al.</i> , 2017).
Pixel Recall (R_p)	$\frac{TP_p}{TP_p+FN_p}$	Proportion of correctly segmented pixels to all pixels in the ground truth.	Cytological examination (overlapping cell segmentation) (Tareef <i>et al.</i> , 2017).
Pixel Accuracy (Acc_p)	$\frac{TP_p+TN_p}{FP_p+FN_p+TP_p+TN_p}$	Pixel level accuracy.	Segmentation of cytoplasm and nuclei (Song <i>et al.</i> , 2015, 2014; Ke <i>et al.</i> , 2021).
Hausdorff Distance	$\max(\sup_{x \in X} d(x, Y), \sup_{y \in Y} d(X, y))$	X and Y are two sets, \sup represents the supremum. It measures the similarity between two point sets.	Cell nuclei segmentation (Kowal <i>et al.</i> , 2020).
Dice coefficient (Dice)	$\frac{2 \times TP}{FP+FN+2TP}$	Dice coefficient is a statistical tool which measures the similarity between two sets of data. It can be used for comparing algorithm output against reference masks.	Semantic instance segmentation of touching and overlapping objects; cytoplasm segmentation; instance segmentation (Böhm <i>et al.</i> , 2019; Wan <i>et al.</i> , 2019; Walter <i>et al.</i> , 2021).
Zijdenbos similarity index (ZSI)	$2 \frac{ R_{GT} \cap R_{Seg} }{ R_{GT} + R_{Seg} }$	R_{GT} and R_{Seg} denote the ground truth and segmented regions, respectively. ZSI computes the ratio of aggregated union between cardinality predicted segmentation output and manual segmentation output.	Overlapping cell segmentation; cervical nuclei segmentation (Tareef <i>et al.</i> , 2017; Hussain <i>et al.</i> , 2020b).
Average Jaccard Index (AJI)	$\frac{\sum_{i=1}^N G_i \cap P_i^M }{\sum_{i=1}^N G_i \cup P_i^M + \sum_{F \in U} P_F }$	G_i is the i -th object from the ground truth with N objects. P_i^M means the M -th connected component in prediction which has the largest Jaccard Index with G_i . AJI measures the ratio of the aggregated intersection and aggregated union for all the predictions and ground truths in the image.	Cell segmentation (Zhou <i>et al.</i> , 2019a).

CRIC (Rezende et al., 2021). The collection CRIC cervix has 400 images of pap smears with 11,534 classified cells. Based on the Bethesda system (Nayar and Wilbur, 2015), CRIC dataset covers conventional cytology cervical cells with six types: NILM (6,779), ASC-US (606), LSIL (1,360), ASC-H (925), HSIL (1,703), and SCC (161).

CDetector (Liang et al., 2021b). This dataset consists of 7,410 cervical images cropped from the WSIs. According to the Bethesda system (TBS), 48,587 object instance bounding boxes are annotated by experienced pathologists which belong to 11 categories: ASC-US, ASC-H, HSIL, LSIL, SCC, atypical glandular cells (AGC), trichomonas (TRICH), candida (CAND), flora, herpes, actinomyces (ACTIN). Till now, CDetector is the largest public dataset for the object detection task in cytology.

Ascites (Su et al., 2020). This dataset is established for screening gastric cancer and collected from Peking University. It consists of 176 H&E stained and Pap stained images cropped from ascites cytopathology images at $40\times$ magnification. A total of 6573 cells (benign and malignant) are annotated using bounding boxes.

RSDC (Ma et al., 2021). It is the only public cytology dataset for developing the refocusing and super-resolution task. The images in the dataset are collected from 5 LBC slides with the resolution $0.243\mu\text{m}/\text{pixel}$. Strategies of bicubic interpolation and gaussian blur are used to generate 15,000 low-resolution images (64×64) and corresponding high-resolution images (128×128) from original slides.

Furthermore, to evaluate the performance of proposed deep learning models, we summarize the evaluation metrics in terms of three canonical DL approaches: classification, detection, and segmentation along with typical cytological applications adopting these metrics, more details are shown in Table 2.

Among these summarized evaluation metrics, classification metrics evaluate the classifier’s capability of predicting the category. Accuracy is the most straightforward metric, yet it ignores the imbalance problem between different categories. The confusion matrix can represent the prediction result of each category. To measure the detection task, *IoU* is a commonly-used metric, which can measure the overlap between the predicted box and the ground truth box. Based on various set thresholds, average precision (*AP*) is utilized to evaluate the performance of the detector in different overlapping levels, including AP_{50} , AP_{75} , etc. Segmentation models can be evaluated by various metrics. For example, *Pixel accuracy* measures the predicted result of each pixel, and *Dice* calculates the similarity coefficient of predicted masks and ground truth.

4. Deep learning in cytology application

In this section, we survey and summarize literatures on various deep learning models applied in computational cytology. Firstly, we introduce preprocessing techniques in cytology image analysis, followed by representative clinical tasks: classification, detection, segmentation, and others. More details of these surveyed literatures are as follows.

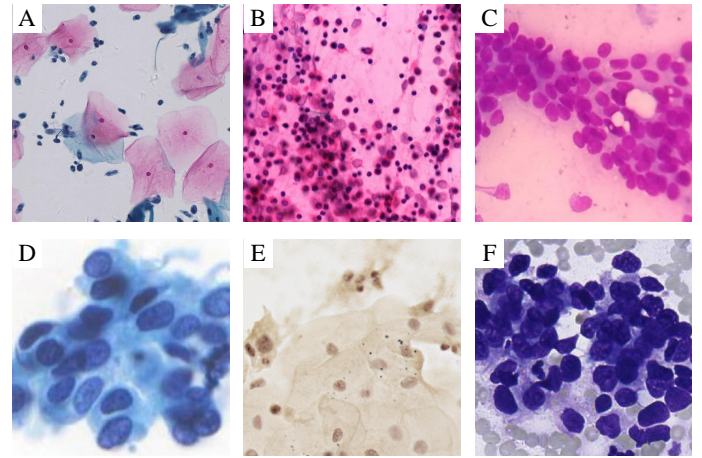


Fig. 8: Staining techniques. (A) Pap (Zhou et al., 2019a). (B) H&E (Su et al., 2020). (C) Giemsa (Bal et al., 2021). (D) Feulgen (Xiang et al., 2020). (E) AgNOR (Amorim et al., 2020). (F) Diff-quick (Gonzalez et al., 2020).

4.1. Preprocessing

Staining techniques. In cytology, staining techniques are introduced to enhance the image features of cells (e.g., texture, structure, and biochemical properties) for visually presenting cellular structures.

Fig. 8 shows various staining techniques in cytology. 1) Pap. As the extensive staining protocols, it has four steps: fixation, nuclear staining, cytosol staining, and transparency. Cell stained by Pap has a clearly-structured nucleus and transparent cytoplasm. According to surveyed literatures, Pap is the most common staining method in cytology images, especially in cervical cancer. 2) Hematoxylin and Eosin (H&E). Hematoxylin stains cell nuclei purplish-blue, and eosin stains the extracellular matrix and cytoplasm pink. In the clinic, H&E is mainly used for staining cells and tissues. 3) Giemsa. It is particularly effective for staining cytoplasm, so Giemsa is mainly used for blood and bone marrow cytological evaluation. Other staining techniques are used for some specific situations. For example, Amorim et al. (2020) stained cervical cells by AgNOR to present cell proliferation, differentiation, and malignant transformation. In another work, Xiang et al. (2020) stained cervical specimens of LBC by Feulgen. Marzahl et al. (2020) stained pulmonary hemosiderophages cytology by Perlss’ Prussian Blue, Turnbull’s Blue.

Stain Normalization. A significant amount of color variations exist in cytology images due to various staining techniques mentioned and other issues (e.g., imaging environment). These differences bring challenges for building robust and generated DL-based cytology models. Besides, normalization can accelerate the convergence when training networks. Therefore, normalization can be a crucial preprocessing step, especially when analyzing stained images, like cytology images, and histopathology images. Commonly-used methods include whitening for removing redundant information from input data, and linear normalization for scaling gray values of input data, etc.

Data augmentation. When the amount of images is not sufficient to learn a robust DL model, especially for medical im-

ages. Data augmentation strategies are introduced to increase the amount of input images for improving the model's generalization. Conventional augmentation methods include geometric transformation (e.g., flipping, rotating, and scaling) and color transformation (e.g., noise, blurring, and contrast). Recently, generative adversarial network (GAN) has been adopted to synthesize a large-scale dataset based on a limited set. Yu *et al.* (2021) utilized GAN to generate 16,000 images from 961 real images for improving cervical cell classification models. In another study, Dey *et al.* (2019) generated 180 images by conditional GAN and learnable class-specific priors for improving classifier performance on cytology tasks. To overcome the data limitation issue, Teramoto *et al.* (2020) proposed a GAN-based augmentation structure, progressive growing of GANs (PGGAN). In this study, real lung cytological images together with synthesized images by PGGAN are used to train classification CNNs, leading to the performance improvements in cytology image classification.

4.2. Classification

In cytology, the DL approaches are feasible and promising for image classification with distinguishable characteristics of cytology samples. The clinical cytologists can distinguish between benign and malignant cells based on their cytological features. For example, the abnormalities are displayed in malignant cells, such as larger and irregular nuclei, enlarged nuclear-cytoplasmic ratio, and the altered shape of the nucleolus. Within cytology image classification tasks, DL-based models aim to extract the underlying patterns of input images for identifying objects (e.g., nucleus, cell) or making slide-level predictions (e.g., cytopathology screening). Therefore, we further divide the cytological classification task into two categories: 1) cell-level, 2) slide-level.

4.2.1. Cell-level classification

Cell-level classification could be one of the most successful tasks in DL-based cytology image analysis (Jantzen *et al.*, 2005). Due to the giga-pixel resolution of collected cytology WSIs, they are usually cut into cell patches for image analysis (Zhang *et al.*, 2019). When training a deep network for classifying cells, cell patches are cropped from these whole images first. Then, these cell patches are fed into DL models to train cell-level classification models after preprocessing.

The most straightforward method is to directly feed cell patches into a multi-layer CNN for extracting feature maps, then crossing the output layer to get the predicted category. A series of CNN-based methods have been proposed. For lung cytology classification, Teramoto *et al.* (2017) designed a deep convolutional neural network consisting of three convolutional layers, three pooling layers, and two fully connected layers. Similarly, Dimauro *et al.* (2019) constructed a three-block CNN model for nasal cell classification. For cervical cytology, Shanthi *et al.* (2019) designed a CNN architecture consisting of three convolutional layers. Its experimental results in different settings (2 class, 3 class, 4 class, and 5 class) showed an effective performance of different grades of cancer in cervical images. In addition, Zhang *et al.* (2017) proposed a simple ConvNet, which was first pre-trained in a natural image dataset,

ImageNet. Then, the model was fine-tuned in two cervical cytological datasets, Herlev and HEMLBC (Jantzen *et al.*, 2005; Zhang *et al.*, 2014), achieving outperforming performance than previous algorithms. However, the performances and generalization capabilities of these simply-designed CNN with several layers are limited to specific datasets and scenarios.

A large amount of advanced deep models are proposed in the computer vision field, such as Inception (Szegedy *et al.*, 2015), ResNet (He *et al.*, 2016) and DenseNet (Huang *et al.*, 2017). These networks can be directly adopted for cytology image analysis and achieve better performance than simply-designed structures in the classification task. For example, Teramoto *et al.* (2019) presented a VGG-based model for classifying benign and malignant cells from lung cytology images. Noyan *et al.* (2020) proposed TzanckNet based on ResNet-50 to identify cells in the cytology of erosive-vesiculobullous diseases. Additionally, some studies compared the performance of advanced CNN architectures in cytology image classification tasks (Sornapudi *et al.*, 2019; Hussain *et al.*, 2020c; Mohammed *et al.*, 2021; Albuquerque *et al.*, 2021). From their experimental results, popular architectures (e.g., ResNet, Inception, and DenseNet) achieved promising performance in cell classification. To provide the interpretability analysis of this CNN-based classification, (Selvaraju *et al.*, 2017) designed Grad-CAM to show region of interests (ROIs) in network decision-making using the gradient information of the last convolution layer of CNN. Teramoto *et al.* (2019) utilized Grad-CAM to generate heatmaps for observing high activation areas on typical regions lung cytology images. By observing the model's high response regions of urothelial cytology images via Grad-CAM, Nojima *et al.* (2021) concluded that the color of tumor nuclei contributes to the prediction of the model most.

Apart from binary classification (i.e., benign and malignant), multi-class scenarios are more common, yet challenging in cytology image analysis, because benign and malignant cells mainly include several sub-categories (Vaickus *et al.*, 2019). For example, Herlev dataset contains 3 types of normal cervical cells and 4 types of abnormal cervical cells (Jantzen *et al.*, 2005). However, the boundaries between the image features of two sub-categories are usually ambiguous, which brings challenges for CNNs to learn distinguishable features. To solve these issues, Lin *et al.* (2019b) proposed a fine-grained classification model for cervical cells. This model introduced mask maps as the morphological appearance information for enhancing fine-grained distinguishable features of cells.

In addition, several cytological studies focus on improving the model's performance in limited or imbalanced datasets. GAN-based models can be utilized to augment original dataset for improving the performance of the classification task. For example, Yu *et al.* (2021) adopted GAN-based data augmentation to improve cervical cell classification models. Dey *et al.* (2019) synthesized 180 images by conditional GAN. Together with the original data, these images are utilized to train three common models (ResNet-152, DenseNet-161, and Inception-V3), achieving significant improvement in FNAC image classification. For the imbalanced dataset problem, the number of positive samples is always far less than the negative ones in

Table 3: Overview of deep learning-based classification studies for computational cytology

Reference	Application	Staining	Organ	Method	Dataset	Result
Cell-level classification						
Zhang <i>et al.</i> (2017)	Cell classification	Pap H&E	Cervix	Data preprocessing (patch extraction, data augmentation) + CNN + Transfer learning (fine-tune)	Herlev; HEMLBC	Herlev: Sens=0.982, Spec=0.983, Acc=0.983, F1=0.988, AUC=0.998; HEMLBC: Sens=0.983, Spec=0.990, Acc=0.986.
Teramoto <i>et al.</i> (2017)	Classification of cancer types (adenocarcinoma, squamous cell carcinoma, and small cell carcinoma)	Pap	Lung	Data augmentation + CNN	Private dataset: 76 images in classes of adenocarcinoma (40), squamous cell carcinoma (20), and small cell carcinoma (16)	Adenocarcinoma: Acc=0.89; Squamous cell carcinoma: Acc=0.600; Small cell carcinoma: Acc=0.703; Total: Acc=0.711.
Dimauro <i>et al.</i> (2019)	Cell classification	Pap	Nasal	Three-block CNN	Private dataset: 3,423 images (cell)	Sens=0.97, Acc=0.99.
Shanthi <i>et al.</i> (2019)	Malignancy detection and classification	Pap	Cervix	Three-layer CNN	Herlev	5-class: Acc=0.941; 4-class: Acc=0.962; 3-class: Acc=0.948; 2-class: Acc=0.957.
Teramoto <i>et al.</i> (2019)	Classification of benign and malignant cells	Pap	Lung	Data augmentation + VGG-16 + GradCAM	Private dataset: 621 images (patch) in classes of benign (306) and malignant (315)	Patch-level: Acc=0.792, AUC=0.872; Case-level: Acc=0.870, AUC=0.932.
Liu <i>et al.</i> (2020)	Classification of cervical squamous lesions	Pap	Cervix	VGG-16	Private dataset: 3,290 images in classes of abnormal cells (1,736) and normal cells (1,554)	Acc=0.9807, P=0.9791, Sens=0.9801, F1=0.9809.
Lin <i>et al.</i> (2019b)	Fine-grained cell classification	Pap	Cervix	Fine-tune + CNN (AlexNet, GoogLeNet, ResNet, and DenseNet)	Herlev	GoogLeNet: Acc=0.945 (2-class), Acc=0.713 (4-class), Acc=0.645 (7-class).
Sornapudi <i>et al.</i> (2019)	Multi-cell classification in liquid-based cytology images	Pap	Cervix	Fine-tune + CNN (ResNet-50, VGG-19, DenseNet-121, Inception-v3)	Herlev; Private dataset: 25 images	ResNet-50: F1=0.8865, AUC=0.95; VGG-19: F1=0.8896, AUC=0.95; Densenet-121: F1=0.8546, AUC=0.94; Inception-v3: F1=0.8072, AUC=0.88.
Hussain <i>et al.</i> (2020c)	Cervical cancer diagnostic prediction	Pap	Cervix	CNN (AlexNet, VGG-16, VGG-19, ResNet-50, ResNet-101, and GoogLeNet)	Herlev	AlexNet: Acc=0.8; VGG-16: Acc=0.8337; VGG-19: Acc=0.8455; ResNet-50: Acc=0.8937; ResNet-101: Acc=0.9450; GoogLeNet: Acc=0.9567.
Mohammed <i>et al.</i> (2021)	Smear classification	Pap	Cervix	10 popular pre-trained CNN	Sipakmed	DenseNet-169: Acc=0.990, P=0.974, R=0.974, F1=0.974.
Albuquerque <i>et al.</i> (2021)	Classification of cervical cancer risk	Pap	Cervix	9 popular CNN	Herlev	Acc=0.756 (7-class), Acc=0.813 (4-class).
Miselis <i>et al.</i> (2019)	Classification of FANC images	H&E	Breast	CNN (AlexNet, GoogLeNet, SqueezeNet, DenseNet, Inception-V3)	Private dataset: 737 images (ROIs from specimens) in classes of benign (275) and malignant (462)	AlexNet: AUC=0.9730; GoogLeNet: AUC=0.9455; SqueezeNet: AUC=0.9152; DenseNet: AUC=0.9244; Inception-V3: AUC=0.9730.
Manna <i>et al.</i> (2021)	Classification of cervical cells	Pap	Cervix	Fuzzy rank + Pre-trained CNN (Inception-V3, Xception and DenseNet-169)	Sipakmed	Acc=0.9855, Sens=0.9852.
Rahaman <i>et al.</i> (2021)	Classification of cervical cells	Pap	Cervix	Hybrid deep feature fusion + CNN (VGG-16, VGG-19, XceptionNet, and ResNet-50)	Sipakmed	Acc=0.9985 (2-class), Acc=0.9914 (3-class), Acc=0.9914 (5-class).
Yu <i>et al.</i> (2021)	Classification of cervical cells	Pap	Cervix	AlexNet + GAN	Private dataset: 22,124 images (cell) in classes of abnormal (1,202) and normal (20,922)	AUC=0.984
Dey <i>et al.</i> (2019)	FNAC cytology image classification	H&E	Breast	Conditional GAN (synthesis) + CNN (ResNet-152, DenseNet-161, Inception-V3)	Private dataset: 150 images in classes of benign (75) and malignant (75)	180 generated images. ResNet-152: Acc=0.7667; DenseNet-161: Acc=0.8667; Inception-V3: Acc=0.8000.
Teramoto <i>et al.</i> (2020)	Classification of cytological images	Pap	Lung	CNN + PGGAN	Private dataset: 511 images (patch) in classes of benign (244) and malignant (267)	Acc=0.853, Sens=0.854, Spec=0.853.
Bakht <i>et al.</i> (2020)	Classification of FNAC images	Pap	Thyroid	CNN (VGG-19, AlexNet) + Transfer learning (Fine-tune)	Private dataset: 9,209 images (cell) in 5 classes	VGG-19: Acc=0.9305; AlexNet: Acc=0.9288.
Vaickus <i>et al.</i> (2019)	Automating the Paris system for cytopathology	Pap	Urine	VGG-19 + Morphometric model	Private dataset: 217 WSIs in classes of negative (51), atypical (60), suspicious (52), and positive (54)	Acc=0.972, Spec=0.976, Sens=0.970.

continued on the next page

Table 3: Overview of deep learning-based classification studies for computational cytology (continued)

Reference	Application	Staining	Organ	Method	Dataset	Result
Kaneko <i>et al.</i> (2021)	Cell image recognition	Pap	Urine	EfficientNet	Private dataset: 4,637 images (cell)	Acc=0.95, Sens=0.97, Spec=0.95, and AUC=0.99.
Žejmo <i>et al.</i> (2017)	Classification of cancer cytological specimen	H&E	Breast	CNN (AlexNet, GoogLeNet)	550 images (ROIs) in classes of malignant (275) and benign (275)	AlexNet: Acc=0.80; GoogLeNet: Acc=0.83.
Shi <i>et al.</i> (2021)	Classification of cervical cells	Pap	Cervix	Graph convolutional Network (GCN)	Sipakmed	Acc=98.37 ± 0.57, Sens=99.80 ± 0.10, Spec=99.60 ± 0.20, F1=99.80 ± 0.10.
Garud <i>et al.</i> (2017)	Classification of FANC cell samples	H&E	Breast	GoogLeNet	Private dataset: 37 images in classes of benign (24) and malignant (13)	Acc=0.8076.
Saikia <i>et al.</i> (2019)	Classification of FNAC images	Pap	Breast	CNN (VGG-16, VGG-19, ResNet-50, and GoogLeNet-V3)	FANC 2019	VGG-16: Acc=0.8867; VGG-19: Acc=0.882; ResNet-50: Acc=0.9056; GoogLeNet-V3: Acc=0.9625.
Nojima <i>et al.</i> (2021)	Diagnose the malignant potential of carcinoma cells	Pap	Urine	Visual geometry group CNN	Private dataset: 203 images	AUC=0.9890, F1=0.9002.
Lilli <i>et al.</i> (2021)	Cell classification	Pap	Urine	VGG-16	Private dataset: 690 images in classes of urothelial normal cells (274) and abnormal cells (416)	Acc=0.899.
Guan <i>et al.</i> (2019b)	Differential diagnosing of papillary thyroid carcinomas	H&E	Thyroid	VGG-16 and Inception-v3	Private dataset: 279 images (thyroid nodules)	VGG-16: 0.9766 (image-level), 0.95 (patient-level); Inception-v3: 0.9275 (image-level), 0.875 (patient-level).
Bal <i>et al.</i> (2021)	Classification of FNAC images	Giemsa H&E	Breast	CNN (13 layers, convolution and fully-connected layers)	Private dataset: Giemsa (1020 images in classes of benign and malignant) and H&E (631 images in classes of benign and malignant)	Giemsa: Acc=0.9781, P=0.977, R=0.973, Spec=0.982, F1=0.975; H&E: Acc=0.9753, P=0.973, R=0.950, Spec=0.987, F1=0.961.
Guan <i>et al.</i> (2019a)	Differential diagnosing of lymph node	H&E	Cervix	Inception-v3	Private dataset: 742 images in 4 classes	Acc=0.8962.
Bhatt <i>et al.</i> (2021)	Cervical cancer detection	Pap	Cervix	EfficientNet + Grad-CAM	Herlev, Sipakmed	Acc=0.9970, P=0.9970, R=0.9972, F1=0.9963, Kappa=0.9931.
Noyan <i>et al.</i> (2020)	Cell identification	Giemsa	Skin	ResNet-50	Private dataset: 2,260 images (Tzanck smear)	Acc=0.943, Sens=0.837, Spec=0.973, AUC=0.974.
Bao <i>et al.</i> (2020)	Detection of cervical intraepithelial neoplasia or invasive cancer	Pap	Cervix	VGG-16	Private dataset: 188,542 images	CIN 2: Acc=0.926; CIN 3+: Acc=0.961.
Sanyal <i>et al.</i> (2018)	Classification of FNAC images	Giemsa Pap	Thyroid	CNN	Private dataset: 370 images in classes of non-PTCA (184) and PTCA (186)	Sens=0.9048, Spec=0.8333, Acc=0.8506.
Wu <i>et al.</i> (2018)	Classification of cancer types	H&E	Cervix	AlexNet	Private dataset: 79 specimens in 3 classes	Acc=0.9333.
Li <i>et al.</i> (2022)	Cervical cell classification	Pap	Cervix	ResNet-50 + Attention mechanism + LSTM	Sipakmed	Sensitivity=0.999, specificity=0.998, F1=0.9989.
Slide-level classification						
Elliott Range <i>et al.</i> (2020)	Classification (prediction of malignancy)	Pap	Thyroid	AlexNet	Private dataset: 908 WSIs	Sens=0.92, Spec=0.905, AUC=0.932.
Dov <i>et al.</i> (2019)	Classification (prediction of malignancy)	Pap	Thyroid	VGG-11 + Multiple instance learning	Private dataset: 908 WSIs	AUC=0.932, AP=0.872.
Tan <i>et al.</i> (2021)	Cervical cancer screening	Pap	Cervix	Faster R-CNN	Private dataset: 408,030 images	Sens=0.994, Spec=0.348, AUC=0.67.
Ke <i>et al.</i> (2021)	Quantitative analysis of abnormalities	Pap	Cervix	U-Net, ResNet-50	Private dataset: 130 WSIs	Segmentation: Pixel Acc=0.974 ± 0.001, IoU=0.913 ± 0.007; Classification: Acc=0.945 ± 0.006.
Cao <i>et al.</i> (2021)	Cancer screening (cell-level detection, patch-level and case-level classification)	Pap	Cervix	Multi-scale region-based CNN + Attention mechanism	Private dataset: 7030 images	Cell-level detection: AP=0.7509; Patch-level classification: AUC=0.9909; Case-level classification: AUC=0.934, Sens=0.913, Spec=0.906 and Acc=0.909.
Li <i>et al.</i> (2021)	High resolution image classification	Pap	Cervix	Mixed supervision learning (image-level + pixel-level)	Private dataset: 862 images from 2 data centers	Center A: Sens=1, Spec=0.86; Center B: Sens=1, Spec=0.87.

continued on the next page

Table 3: Overview of deep learning-based classification studies for computational cytology (continued)

Reference	Application	Staining	Organ	Method	Dataset	Result
Dov <i>et al.</i> (2021)	Classification (prediction of malignancy)	Pap	Thyroid	MIL+ NoisyAND + Attention mechanism + Maximum likelihood estimation	Private dataset: 142 WSIs with 4,494 instances	AUC=0.870 \pm 0.017, AP=0.743 \pm 0.037.
Gonzalez <i>et al.</i> (2020)	Distinguish large cell neuroendocrine	Pap, H&E, Diff-Quik	Lung	CNN	Private dataset: 40 images in high-grade neuroendocrine carcinoma (17 small cell, 13 large cell, 10 mixed/unclassifiable)	H&E: Acc=0.900; Pap: Acc=0.875; Diff-Quik: Acc=0.889.
Zhu <i>et al.</i> (2021)	Rapid TBS classification of cervical liquid-based thin-layer cell smears	Pap	Cervix	Model assembly: Xception (classification), YOLOv3 (object detection), and U-Net (segmentation)	Private dataset: 81,727 images	Speed=180s/slide, Sens=0.9474.
Wei <i>et al.</i> (2021)	Cervical lesion detection, WSI-level classification of normal and abnormal	Pap	Cervix	YOLOv3 + Transformer	Private dataset: 2,019 images (slide) from four scanning devices	AUC=0.872.
Cheng <i>et al.</i> (2021)	WSI-level cervical cancer screening	Pap	Cervix	CNN (ResNet50) + RNN	Private dataset: 3,545 images (slide) with 79,911 annotations	Spec=0.935, Sens=0.951, Speed=1.5min/slide.
Awan <i>et al.</i> (2021)	Cell-level classification, WSI-level risk stratification	Pap	Urine	RetinaNet + Counting of atypical and malignant cells	Private dataset: 398 images (slide) in classes of normal (243), inflammatory (13), CA (76), ASM (38) and TCC (28)	Cell-level classification: AUC=0.99; Risk stratification: AUC=0.83.
Lin <i>et al.</i> (2021)	Smear-level risk stratification	Pap	Cervix	CNN with dual-path encode + Synergistic grouping loss	Private dataset: 19,303 WSIs (13,486 for training, 2,486 for validation and 3,331 for testing) from 4 centers in 6 classes of cells	Sens=0.907, Spec=0.80, AUC=0.925.

cytological scenarios (Yu *et al.*, 2021; Bakht *et al.*, 2020). A few studies employed sampling techniques to balance different classes (Li *et al.*, 2019; Bakht *et al.*, 2020). For learning-based solutions, Yu *et al.* (2021) adopted GAN to balance different classes by synthesizing images for those classes with far less amount than others.

Recently, some other advanced methods have been investigated for cytology classification. Li *et al.* (2022) introduced an attention mechanism block to guide the network to focus on cell areas, thus improving the capability of extracting deep features. Then, they added a pyramid pooling layer and a long short-term memory module (LSTM) to aggregate image features in different regions. To improve the classification performance, Shi *et al.* (2021) proposed a cervical cell classification method based on graph convolutional network (GCN), which can explore the potential relationship of cervical cell images.

In clinic practice, DL-based classification approaches have been widely applied for various types of cancers, including cervix (Shanthi *et al.*, 2019), breast (Miselis *et al.*, 2019), lung (Teramoto *et al.*, 2017), thyroid (Bakht *et al.*, 2020), urine (Vaickus *et al.*, 2019), nasal (Dimauro *et al.*, 2019) and skin (Noyan *et al.*, 2020). Specifically, Vaickus *et al.* (2019) proposed a VGG-based model for classifying urine cytopathology images. Bakht *et al.* (2020) developed a VGG-based model for thyroid nodule cell classification. For cervical cytology, Bao *et al.* (2020) compared AI-assisted techniques with skilled cytologists in detecting cervical intraepithelial neoplasia or invasive cancer. For skin cytology, Noyan *et al.* (2020) proposed a ResNet-based model to identify cells in the cytology of erosive-vesiculobullous diseases. These studies demonstrated the substantial clinical value of classification-assisted cytology

image analysis.

4.2.2. Slide-level classification

Different from cell-level classification, the goal of the slide-level classification model is to predict the category of whole images instead of cell samples.

Giga-pixel WSI classification systems are being investigated for efficient and high-accuracy predictions. Some studies built slide-level classification systems by multi-stage designs. For example, Cheng *et al.* (2021) designed a robust and progressive WSI analysis method for cervical cancer screening. In the first stage, the authors developed a progressive lesion cell recognition method combining low- and high-resolution WSIs. Then, a RNN-based WSI classification model was built for WSI-level predictions in the second stage. In another slide-level study, Wei *et al.* (2021) designed a lightweight model (YOLCO) based on YOLO series (Redmon *et al.*, 2016) to make local predictions (e.g., cell-level, patch-level) in the first stage, which can enrich the multi-scale connectivity by additional supervision of spatial information. In the second stage, these local predictions were input to a transformer architecture for WSI-level results. Its experimental results showed that the framework presented a higher AUC score and 2.51 \times faster than the state-of-the-art methods in WSI classification. For accurate and efficient screening of cervical cancer, Zhu *et al.* (2021) developed a complete cervical LBC smear TBS diagnostic system. This system integrated XGBoost and a logical decision tree with three typical DL models, i.e., Xception for classification, YOLOv3 for object detection, and U-Net for segmentation. This diagnostic system can reduce cytologists' workload, improve the accuracy of cervical cancer screening.

Weakly supervised learning strategies are introduced to learn information from limited annotations in slide-level classification. Weakly supervised learning is appealing for this scenario. For example, [Dov et al. \(2021\)](#) presented a MIL model for thyroid cancer malignancy prediction from cytopathology images. Then, an attention module was integrated into this MIL-based model with maximum likelihood estimation (MLE) architecture. The experimental results showed the competitive performance in thyroid malignancy prediction. [Li et al. \(2021\)](#) developed mixed supervision learning for WSI classification by effectively utilizing their various labels (e.g., sufficient image-level coarse annotations and a few pixel-level fine labels).

By introducing advanced strategies or designs, quite a few cytology studies investigated to improve classification performance. For example, [Cao et al. \(2021\)](#) integrated the attention module into multi-scale region-based CNN (feature pyramid network) between upsampling and downsampling pathway. Three experiments in different levels consisting of cell-level detection, patch-level, and case-level classification demonstrated the effectiveness of the introduced attention mechanism. Other studies designed different auxiliary tasks (e.g., detection, segmentation) to assist the classification task. [Tan et al. \(2021\)](#) employed an object detection model (Faster R-CNN) to assist classification for cancer screening. [Ke et al. \(2021\)](#) introduced U-Net for improving the classification of squamous cell abnormalities.

Risk stratification is one important task of slide-level classification, which determines the risk level of patients suffering from diseases. [Awan et al. \(2021\)](#) designed a DL-based digital cell profile for risk stratification of urine cytology images. In this system, RetinaNet was adopted for cell-level classification and detection in the first stage. For WSI-level risk stratification, they identified low-risk and high-risk cases using the count of atypical cells and the total count of atypical and malignant cells. [Lin et al. \(2021\)](#) presented a dual-path network for cervix risk stratification, which can be divided into two steps. Firstly, an efficient CNN with a dual-path encoder was proposed for lesion retrieval, which can ensure the inference efficiency and sensitivity on both tiny and large lesions. Then, a smear-level classifier (rule-based risk stratification) was introduced to align reasonably with the intricate cytological definition of the classes. Extensive experiments on a huge dataset consisting of 19,303 WSIs from multiple medical centers validated the robustness of this risk stratification method.

4.3. Detection

In cytology image analysis, developing automatic detection methods to find tiny objects (e.g., malignant cells and nuclei) in the whole image is crucial to reduce experts' tedious and time-consuming workflow. DL-based object detection has achieved significant progress in medical image analysis, which can be divided into two categories: 1) One-stage method, which directly regresses the category and location of instance objects in a single architecture. 2) Two-stage method, which firstly predicts object candidates in the first stage and then classifies and localizes them in the second stage.

4.3.1. One-stage methods

One-stage algorithms detect objects by directly generating the category and coordinates of objects with the advantages of high detection efficiency, such as SSD ([Liu et al., 2016](#)), YOLO ([Redmon et al., 2016](#)), and RetinaNet ([Lin et al., 2017b](#)).

Many works in cytology introduce the YOLO model as their base network due to its high efficiency. For the structure of YOLO, it divides the original image into an $S \times S$ grid cell. Then, YOLO predicts bounding boxes, confidence for each cell. Afterwards, redundant boxes are removed by the confidence threshold and non-maximum suppression. [Xiang et al. \(2020\)](#) used YOLO as their detector for cervical cells. Similarly, [Kilic et al. \(2019\)](#) adopted YOLO to detect nuclei in pleural effusion cytology. The authors compared the detection efficiency between one-stage and two-stage detectors ([Ren et al., 2015](#)). Its experimental result showed that YOLO achieved a test speed of 0.060 second/image that was much faster than 1.627 second/image in Faster R-CNN (two-stage detector). Besides, [Moosavi Tayebi et al. \(2021\)](#) applied YOLO on selected appropriate ROI tiles to automatically detect and classify bone marrow cellular and non-cellular objects. To improve the performance of YOLO in cervical cell detection, [Liang et al. \(2021a\)](#) proposed a global context-aware framework by introducing an image-level classification branch and a weighted loss that can filter false positive predictions.

To improve the feature extractor for learning multi-scale features, RetinaNet was proposed by using feature pyramid network (FPN) as its feature extractor, which achieved the state-of-the-art detection performance ([Lin et al., 2017a](#)). [Marzahl et al. \(2020\)](#) employed RetinaNet for generating rich and multi-scale features for functional head (e.g., box, regression, and classification). These results contributed to the quantification of pulmonary hemosiderophages in this work.

4.3.2. Two-stage methods

Two-stage methods use different region proposal strategies to generate bounding boxes, such as sliding windows ([Girshick, 2015](#)), selective search ([Van de Sande et al., 2011](#)), and region proposal network ([Ren et al., 2015](#)). For example, Fast R-CNN designed selective search strategy to generate bounding boxes. Then, the ROI pooling layer extracts the features of each ROI. Fast R-CNN outputs softmax probabilities and per-class bounding-box regression offsets with a multi-task loss ([Girshick, 2015](#)). To integrate different modules and increase the speed ([Ren et al., 2015](#)), Faster R-CNN improves Fast R-CNN by integrating feature extraction, proposal, bounding box regression, and classification. It designs region proposal networks (RPN), which uses bounding box regression for accurate region proposal.

To detect cell objects in the whole cytology image, some studies employed Faster R-CNN as their base architecture. For example, [Li et al. \(2019\)](#) utilized Faster R-CNN to detect cervical exfoliated cells on the LBC dataset. Similarly, Faster R-CNN was also used to detect tumor cells for further classification, which formed an ascites cytopathology image interpretation system ([Su et al., 2020](#)).

For different cytological scenarios, researchers improved de-

Table 4: Overview of deep learning-based detection studies for computational cytology

Reference	Application	Staining	Organ	Method	Dataset	Result
One-stage methods						
Kilic et al. (2019)	Nuclei detection	Pap	Pleural effusion	YOLOv3	Private dataset: 200 images with 11,157 nuclei	Precision: 0.941, Recall=0.9898, F1=0.9648, Test time=0.060 sec/img.
Xiang et al. (2020)	Automation-assisted cervical cancer reading	Feulgen	Cervix	YOLOv3	Private dataset: 12,909 images with 58,995 ground truth boxes in 10 categories	Detection: mAP=0.602; Classification: Sens=0.975, Spec=0.687.
Moosavi Tayebi et al. (2021)	Hematological diagnosis	Giemsa	Bone marrow	YOLOv4	Private dataset: 75,000 annotated tiles of bone marrow aspirate	Region detection: Acc=0.97, AUC=0.99; Cell detection: mAP=0.75, F1-score=0.78.
Liang et al. (2021a)	Cell detection	Pap	Cervix	Global context-aware + Soft scale anchor matching	Private dataset: 12,909 cervical images with 58,995 ground truth boxes corresponding to 10 categories objects	mAP=0.6544.
Two-stage methods						
Li et al. (2019)	Cell detection and classification	Pap	Cervix	Faster R-CNN + Transfer learning	Private dataset: 680 LBC cervical exfoliated cell samples	Classification: Acc=0.9161 Detection: mAP=0.6698.
Hossain et al. (2019)	Nuclei detection, Estimate proliferation rate	H&E	Kidney	R-CNN	Private dataset: 16,905 segmented cancer cell and 22,948 normal cell nuclei	P=0.9901, R=0.9870, F1=0.988.
Pirovano et al. (2021)	Localization and detection of abnormalities	Pap	Cervix	Weakly supervised CNN + Regression constraint	Herlev	Severity classification: Acc=0.952; Normal/abnormal classification: Acc=0.952, KAPPA score=0.870; Detection: Acc=0.804.
Chai et al. (2021)	Cell detection	Pap	Cervix	Faster R-CNN + Deep metric learning	Private dataset: 240,860 images	100% labeled: mAP=0.27; 75% labeled: mAP=0.254; 50% labeled: mAP=0.195.
Su et al. (2020)	Ascites cytopathology interpretation	Pap, H&E	Stomach	Classification: pre-trained AlexNet, VGG-16, GooleNet, ResNet18, and ResNet-50. Detection: Faster R-CNN	Ascites 2020	Classification: AUC=88.51 (ResNet50); Detection: IoU=0.8722, mAP=0.8316.
Xie et al. (2018)	Cell detection	H&E	Cervix	Fully residual CNN + Structured regression	HeLa cervical cancer	Precision=0.98, Recall=0.98, F1=0.98.
Marzahl et al. (2020)	Quantification of pulmonary hemosiderophages	Prussian turn-bull	Lung	ResNet-18, FPN	Private dataset: 17 WSIs with 78,047 hemosiderophages	Concordance=0.85, mAP=0.66.
Zhang et al. (2019)	Cervical cytology analysis	Pap	Cervix	Lesion cell detection: Faster R-CNN and RetinaNet. Cell type classification: Inception-v3, ResNet-101, and DenseNet-121	Private dataset: 1,167 WSIs with 14,432 image patches, and 27,972 labeled lesion cells	Detection: mAP=0.2116 (Faster R-CNN); Classification: Acc=0.8884, F1=0.5996 (DenseNet-121).
Liang et al. (2021b)	Cervical cancer screening (cell/clumps detection)	Pap	Cervix	Faster R-CNN + Few-shot learning + Prototype representation	CDetector	mAP=0.488.
Baykal et al. (2020)	Nuclei detection	Pap	Pleural effusion	Detector: Faster R-CNN, R-FCN and SSD	Private dataset: 200 images (11,157 nuclei)	Faster R-CNN (ResNet-101): F1=0.9812.

tection performance by modifying architectures or integrating with other strategies ([Hossain et al., 2019](#); [Marzahl et al., 2020](#)). For efficient cell and robust detection, [Xie et al. \(2018\)](#) presented a structured regression model based on a proposed fully residual CNN. This model produced a dense proximity map that exhibited higher responses at locations near cell center. Then, training this model only required annotations of the dot instead of the traditional box, which can improve efficiency of annotating. Several studies paid attention to weakly supervised learning settings in cytological detection. For example, [Pirovano et al. \(2021\)](#) proposed a computer-aided diagnosis tool for cervical cancer screening. In this method, the authors designed a weakly supervised localization strategy, which performed the Integrated Gradient method ([Sundararajan et al., 2017](#)) to com-

pute attribution maps and morphological operations to obtain the localization boxes. In another work, [Chai et al. \(2021\)](#) proposed a semi-supervised deep metric learning method to improve intra-class feature compactness for cervical cancer cell detection. This model learned an embedding metric space and conducted dual alignment of semantic features on both the proposal and prototype levels. From their quantitative experiments, detection of cervical cancer cell can be a challenging study, especially for some cell classes, like ASC-US.

The clinic practice not only requires high detection accuracy but also efficiency because faster detection speed is more suitable for large-scale screening scenarios ([Lin et al., 2019a](#)). Detection models usually face trade-offs between the accuracy and the speed. For example, two-stage detectors (e.g., Faster R-

CNN) can achieve higher detection results while one-stage detectors (e.g., YOLO) have advantages in faster detection speed. In cytological studies, Zhang *et al.* (2019) compared the performance between two-stage (Faster R-CNN) and one-stage (RetinaNet) methods for the detection of cervical lesion cells. The results showed that the former one achieved better experimental results in average precision. In another work (Liang *et al.*, 2021b), the authors improved Faster R-CNN and compared it with baseline and RetinaNet in a limited data scenario. The results in cervical cell/clumps detection showed that RetinaNet (one-stage) achieved significantly faster speed (FPS). Baykal *et al.* (2020) compared three detectors, i.e., Faster R-CNN (two-stage), R-FCN (two-stage), and SSD (one-stage). As a result, R-FCN achieved a higher mAP score while SSD spent less time when testing. Their experimental results validated the trade-offs of these detection models between speed and accuracy.

4.4. Segmentation

The segmentation task aims at morphologically delineating the object contour. For segmentation models, they assign each pixel of the image to a specific category, so it can be regarded as a pixel-wise classification task. In cytological screening, segmentation is an essential step for different applications, including 1) separating cells/clump and background from specimens, 2) morphologically distinguishing cell types, 3) accurately segmenting cellular structures, such as nuclei and cytoplasm.

The main challenge of cytology segmentation is accurately segmenting overlapping areas between cells (Lu *et al.*, 2015, 2016). To address this issue, there are mainly two solution schemes. One is dividing the cytological segmentation task into two stages. The first stage is to utilize a semantic segmentation model (e.g., U-Net) for a coarse result, followed by a series of refinement designs for overlapping areas, thus obtaining the final accurate segmentation result. The other is based on the detect-then-segment paradigm (e.g., Mask R-CNN), which detects cytology objects in whole images and output a segmentation map by mask prediction head. This type of approach can segment objects from each detected instance in an end-to-end architecture without any refinement design. Therefore, we divide the solutions of cytology segmentation into two categories: 1) segment-then-refine method, 2) detect-then-segment method.

4.4.1. Segment-then-refine method

Cytological structures can be segmented by segmentation models, like U-Net. However, overlapping areas belonging to several cells bring defiance of accurately segmenting each cell structure. To overcome this issue, different refinement strategies are proposed to add after the coarse segmentation model for fine-level segmentation.

The segmentation network was originally implemented by establishing a pixel-wise classification network through CNN. Song *et al.* (2015) designed a multi-scale convolutional network for coarse segmentation. Kowal *et al.* (2020) proposed a more complex CNN structure consisting of four convolutional layers, two max-pooling layers, and one fully connected layer. This architecture was utilized in the first stage for nuclei segmentation in cytological images.

Afterwards, U-Net almost replaces the previous pixel-level classification network after its occurrence, especially in biomedical image segmentation (Ronneberger *et al.*, 2015). U-Net is a downsampling-upsampling structure with skip connections for combining low-level and high-level features. Recently, U-Net has made great achievements in medical image segmentation. For example, Falk *et al.* (2019) designed U-Net for cell counting, detection, and segmentation. This work illustrated its potential for cellular structure analysis. In cytology image segmentation, U-Net has been introduced as the backbone for segmenting cellular objects in various cytology, such as oral (Matias *et al.*, 2021), cervix (Araujo *et al.*, 2019), and breast (Kowal *et al.*, 2020). Several works focus on improving the performance of U-Net to enhance their capacities of cell segmentation. For instance, Böhm *et al.* (2019) proposed to mix 2D and 3D U-Net for semantic instance segmentation of touching objects. Zhang *et al.* (2020) introduced attention mechanism to improve U-Net for focusing on ROIs. Besides, Husain *et al.* (2020b) improved U-Net by adding residual blocks, densely connected blocks, and a fully convolutional layer as a bottleneck between encoder-decoder blocks for nuclei segmentation in cervical images.

In segment-then-refine methods, the second stage is to address the issue of overlapping and refine segmentation results. Most of them take the shape prior of cell into considerations. For instance, Song *et al.* (2016) proposed a dynamic multi-template deformation model together with high-level morphological constrain for further boundary refinement. Kowal *et al.* (2020) designed a series of refinement strategies in the second stage: conditional erosion for determining nuclei seeds, the seeded watershed for separation overlapping nuclei, and aggregating segmentation results for overlapping and non-overlapping nuclei. In addition, Zhang *et al.* (2020) proposed a graph-based random walk method for extracting both nucleus and cytoplasm of overlapping cervical cells. This method utilized polar coordinate sampling for removing fake nuclei. Its experimental results in ISBI 2014 dataset showed the performance improvement on extracting an individual cell from heavy overlapping cell clumps. Walter *et al.* (2021) proposed to predict object probability, star distance, and overlap probability based on U-Net. Then, non-maximum suppression was used to generate overlapping cell segmentation results. These refinement strategies can achieve more accurate segmentation results, especially for overlapping regions. However, complex clinical data will present more challenges to the reproducibility and generalizability.

In addition, some other models have been proposed for cytological segmentation. Tareef *et al.* (2017) designed a two-stage segmentation model, which consists of initial segmentation based on Voronoi diagram, and final segmentation with learning shape prior model. In order to segment overlapping cervical cytoplasm, Song *et al.* (2020) proposed a shape mask generator to refine shape priors. Wan *et al.* (2019) presented an architecture for cell detection and cytoplasm segmentation. In this method, conditional random field algorithm (CRFs) and cell boundary refinement were utilized to achieve accurate segmentation of overlapping cells in cervical cytology.

Table 5: Overview of deep learning-based segmentation studies for computational cytology

Reference	Application	Staining	Organ	Method	Dataset	Result
Segment-then-refine methods						
Falk <i>et al.</i> (2019)	Cell counting, detection, and morphometry	Fluorescence	Various	U-Net	ISBI cell tracking 2015	IoU=0.9203 (PhC-U373), IoU=0.7756 (DIC-HeLa).
Matias <i>et al.</i> (2021)	Segmentation, detection, and classification of cell nuclei	Pap	Oral	Classification: ResNet-34. Detection: Faster R-CNN. Segmentation: U-Net	Oral 2021	Classification: Acc=0.88, F1=0.86; Detection: IoU=0.5832; Segmentation: IoU=0.4607.
Song <i>et al.</i> (2014)	Segmentation of cytoplasm and nuclei	H&E	Cervix	CNN+ Coarse to fine segmentation	Private dataset: 53 slides with 1400 cells	Nuclei region detection: Acc=0.9450, F1=0.9453; Segmentation: F1=0.8951±0.0215.
Song <i>et al.</i> (2015)	Segmentation of cytoplasm and Nuclei	H&E	Cervix	Multi-scale CNN + Graph partitioning + Touching cell splitting	Private dataset: 53 images (slide)	Cytoplasm: Dice=0.95; Nuclei: Dice=0.99.
Song <i>et al.</i> (2016)	Cell segmentation	Pap H&E	Cervix	Multi-scale CNN + Dynamic multi-template deformation	ISBI 2015. Private dataset: 21 images (each image has 30~80 cells)	ISBI 2015: Dice=0.89; Private dataset: Dice=0.84.
Araujo <i>et al.</i> (2019)	Cell image segmentation and ranking	Pap	Cervix	CNN	BHS 2019	Segmentation: P=0.73, R=0.65, F1=0.69, Time=4.75s; Ranking: mAP=0.936.
Kowal <i>et al.</i> (2020)	Cell nuclei segmentation	H&E	Breast	CNN + Seeded watershed	Public dataset: 80 images	Benign: Hausdorff distance=0.840, Jaccard distance=0.776; Malignant: Hausdorff distance=0.781, Jaccard distance=0.732.
Böhm <i>et al.</i> (2019)	Semantic instance segmentation of touching and overlapping objects	Pap	Cervix	U-Net	OSC-ISBI	Dice=0.895±0.079.
Zhang <i>et al.</i> (2020)	Cervical cell segmentation	Pap	Cervix	Attention mechanism + U-Net + Random walk	ISBI 2014	Nuclei: $P_p=0.94 \pm 0.06$, $R_p=0.95 \pm 0.05$, Dice=0.93 ±0.04; Cytoplasm: $TP_p=0.94 \pm 0.06$, $FP_p=0.003 \pm 0.004$, Dice=0.93 ±0.07.
Walter <i>et al.</i> (2021)	Instance segmentation	Pap	Cervix	U-Net + Star-convex polygons	OSC-ISBI	Dice=0.85 ± 0.07.
Hussain <i>et al.</i> (2020b)	Segmentation and classification of cervical nuclei	Pap	Cervix	U-Net	Herlev	Classification: Acc=0.988; Segmentation: ZSI=0.97.
Tareef <i>et al.</i> (2017)	Cytological examination (overlapping cell segmentation)	Pap	Cervix	CNN+ Shape prior (dynamic shape modeling)	ISBI 2014	Nuclei: $P_p=0.94 \pm 0.06$, $R_p=0.95 \pm 0.06$, ZSI=0.94 ±0.04; Cytoplasm: ZSI=0.90 ±0.08.
Song <i>et al.</i> (2020)	Overlapping cytoplasm segmentation	Pap H&E	Cervix	Shape mask generator + Refining shape priors	ISBI 2015. Private dataset: 160 clumps with 962 cytoplasm	Pap: Dice=0.854 ± 0.049; H&E: Dice=0.846 ± 0.054.
Wan <i>et al.</i> (2019)	Nuclei detection, cytoplasm segmentation	Pap	Cervix	CNN + Double-window + Image processing + Deeplab V2 + CRFs + Cell boundary refinement	ISBI 2014; ISBI 2015; Private dataset: 580 image (patch)	ISBI 2014: Dice=0.93 ± 0.04; ISBI 2015: Dice=0.92 ± 0.05; Private: Dice=0.92 ± 0.04.
Detect-then-segment methods						
Sompawong <i>et al.</i> (2019)	Pap smear cancer screening	Pap	Cervix	Mask R-CNN + Fine-tuning	Private dataset: 178 images in classes of normal (2,734), atypical (494), low-grade (148), and high-grade cells (84)	Image-level: mAP=0.578, Acc=0.917, Sens=0.917, Spec=0.917; Nucleus: Acc=0.898, Sens=0.725, Spec=0.943.
Zhou <i>et al.</i> (2019a)	Cell segmentation	Pap	Cervix	PRN + Cell association matrix	Private dataset: 413 images (annotated 4,439 cytoplasm and 4,789 nuclei)	Cytoplasm: AJI=0.7185, F1=0.7497; Nuclei: AJI=0.5496, F1=0.7554.
Zhou <i>et al.</i> (2020)	Cell instance segmentation	Pap	Cervix	RPN + Knowledge distillation	Private dataset: 413 labeled (4,439 cytoplasm and 4,789 nuclei) and 4,371 unlabeled images	100% labeled: AJI=0.6643, mAP=40.52; 80% labeled: AJI=0.6692, mAP=0.4013; 40% labeled: AJI=0.6449, mAP=0.3726.

4.4.2. Detect-then-segment method

For the segmentation of instance objects in cytology images, these methods follow the detect-then-segment paradigm, which divides this task into two steps: detecting all objects in whole

images, then segmenting instances from each detected object. As one popular architecture of this paradigm, Mask R-CNN improves Faster R-CNN by adding full connected layers as the segmentation head. Thus, it can output the prediction of clas-

Table 6: Overview of deep learning-based studies of other tasks for computational cytology

Reference	Application	Staining	Organ	Method	Dataset	Result
Ma <i>et al.</i> (2020)	Super resolution	Pap	Cervix	Image registration + GAN	Private dataset: 142 WSIs (118 for training and 24 for testing) with 174,500 patches	PSNR=26.92, SSIM=0.88, MOS=3.80.
Ma <i>et al.</i> (2021)	Super resolution	Pap	Cervix	Backbone + Self-texture + Flexible reconstruction	Public dataset: 5 slides (25,000 patches)	PSNR=35.47, SSIM=0.958, MSE=22.07.
Teramoto <i>et al.</i> (2021)	Mutual stain conversion	Giemsa and Pap	Lung	CycleGAN	Private dataset: 191 Giemsa-stained images and 209 Papanicolaou-stained images	T test: P-value <0.001.

sification, detection, and segmentation via a single architecture (He *et al.*, 2017; Ren *et al.*, 2015).

Instance segmentation is regarded as one of the most challenging tasks in cytology image analysis, because it not only predicts the instance morphology but also distinguishes different instances (e.g., cytoplasm, nucleus). Building detect-then-segment models can solve this problem, since they can predict instance detection and segmentation results through a single architecture. A few studies investigated this category of cytological segmentation methods. Existing researches almost employ Mask R-CNN as their architecture, because there is no need for further design of overlapping areas in this category of methods. For example, Sompawong *et al.* (2019) adopted Mask R-CNN for specifying the bounding box, nucleus mask, and class of each cervical cell. In another study (Zhou *et al.*, 2019a), authors utilized the multi-head attention mechanism to explore instance-level association by propagating features based on attention scores. Consequently, this proposed model improved the instance representation and achieved better instance segmentation performance than original Mask R-CNN. To further reduce reliance on large amounts of labeled data, Zhou *et al.* (2020) proposed a semi-supervised learning approach to leverage both labeled and unlabeled data for instance segmentation by knowledge distillation.

4.5. Other tasks

In addition to the typical deep learning tasks, i.e., classification, detection, and segmentation, a few other tasks of cytology image analysis have also been investigated, such as super-resolution (SR), and stain conversion (Table 6). In the cytopathology screening, low-resolution and out-of-focus images will harm the decision-making process of cytologists, thus high-resolution digital cytopathology slides are the prerequisite for the interpretation of lesion cells. To control the image quality, super-resolution models are designed to generate high-resolution images. Ma *et al.* (2020) introduced a GAN-based progressive multi-supervised super-resolution model (PathSRGAN) to learn the mapping of real low-resolution and high-resolution images. After that, they designed a self-texture transfer super-resolution and refocusing network (STSRNet) to reconstruct HR multi-focal plane (MFP) images from a single 2D low-resolution (LR) wide field image (An *et al.*, 2021). As mentioned in section 4.1, different staining methods are used to observe different cell structures and components. DL-based stain conversion can be used for staining normalization and eliminate data heterogeneity issues. Teramoto *et al.* (2021) proposed

a CycleGAN-based style transfer model for stain conversion between Giemsa-stained and Pap-stained images. This study performed visual evaluations of the authenticity of cell nuclei, cytoplasm, and cell layouts of synthetic lung cytology images.

5. Challenges and Promises

Despite great advancements and improvements in computational cytology over the last few years, there are still quite a few challenges and opening problems that are waiting to be resolved. Meanwhile, the development of deep learning technologies and pathology is continuously bringing vigor and vitality into this emerging field. In this section, we further discuss prospects and potential research directions of computational cytology.

5.1. Label-efficient learning with limited annotations

Data is regarded as the prerequisite of learning-based methods, because it is hard to develop effective models without good quality datasets (Falk *et al.*, 2019; Jónsson *et al.*, 2019). In medical image analysis, large-scale labeling can be a heavy burden for cytologists, because they need to first manually delineate ROIs in WSIs, then annotate each object (e.g., nucleus, cell, and cluster) in these ROIs by the box or mask. Compared with the extensive dataset in histopathology (such as TCGA (Tomczak *et al.*, 2015)), public datasets of cytology are more limited not only in their numbers, but also in cancer types and annotation types (see in Table 1). Therefore, how to efficiently utilize datasets with limited annotations can be challenging for developing cytological analysis models (Dov *et al.*, 2021; Chai *et al.*, 2021).

In recent years, the concept of label-efficient learning is proposed to make full use of the limited annotations for leveraging information, including semi-supervised learning, multiple instance learning, mixed supervised learning, etc. Specifically, semi-supervised learning aims to solve this problem by learning knowledge from both labeled data and unlabeled data. Recently, Zhou *et al.* (2020) designed a semi-supervised learning method by a mask-guided teacher-student framework for overlapping cell instance segmentation. Another learning scheme, MIL utilizes image-level annotations for instance-level tasks, which has been investigated in the field of medical image analysis, especially for histopathology. Recently, Dov *et al.* (2021) proposed a MIL-based algorithm in thyroid cytology, which can simultaneously predict multiple bag and instance-level labels

for thyroid malignancy prediction from WSIs. However, the potential of MIL in pap smear image and other cytology images remains to be explored. As illustrated in Table 1, there are usually different annotation types in different datasets, including box, mask, and the image-level label. Recently, mixed supervised learning gains popularity in analyzing images with different types of annotations. It has been demonstrated as an effective learning scheme in medical domain. For example, Luo *et al.* (2021) present a deep omni-supervised thoracic disease detection network from chest X-rays with massive image-level annotations and scarce lesion-level annotations. This learning paradigm can substantially reduce the demand for fine annotation, thus reducing workload of doctors significantly.

In addition to the effective utilization of annotations, it is also promising to build efficient labeling approaches for reducing the burden on annotators. For example, introducing human knowledge into the loop of annotation can effectively and actively obtain accurate and credible annotations. Koohbanani *et al.* (2020) proposed an annotating method named NuClick with a squiggle as a guiding signal, enabling it to segment the glandular boundaries. However, this method still requires human full attention to annotate samples, which is a huge cost for society and tedious for human experts. For cytology images, they always contain numerous cells, especially in giga-pixel WSIs, how to establish an effective labeling process remains largely unexplored.

5.2. Fine-grained classification and morphological feature characterization

Although various deep learning applications have been developed in cytology image analysis (e.g., classification, detection, and segmentation), some of these tasks are worthy of further investigation, such as fine-grained classification for cancer diagnosis and instance segmentation in overlapping cell scenarios.

As a fundamental task, cytological classification aims to distinguish between benign and malignant cells. However, there are many types of cells with varying degrees of cancerization. For example, the types of cervical cells include squamous cells and glandular cells, and they can be further subdivided into sub-categories (Nayar and Wilbur, 2015). Besides, each type of cell has large intra-variance and small inter-variance. These factors bring significant challenges to deep feature extractors for learning distinguishable features. Further fine-grained classification of malignant cells can solve these problems and assist cytologists in accurate cancer diagnosis. Zhang *et al.* (2019) demonstrated the difficulty of fine-grained tasks compared to coarse-grained tasks. In their experiments, the classifier of cervical cytology showed significantly worse performance of fine-grained than coarse-grained tasks. Some studies introduced additional information and prior to learn fine-grained feature representations. For example, Lin *et al.* (2019b) built a fine-grained classification model for distinguishing cervical cells. The authors introduced cytoplasm and nucleus masks as morphological information to extract fine-grained features. Therefore, fine-grained feature extractors for learning subtle feature diversity are essential for cytology image analysis.

Another fundamental application, instance-level segmentation of cytoplasm and nucleus can be used to calculate the

nuclear-cytoplasmic ratio, which is an essential indicator for distinguishing malignant cells. However, cell overlapping brings challenges for accurately instance segmenting cellular structures (Song *et al.*, 2014, 2015). A large amount of studies focus on this challenge, and most of them divide this task into two stages: semantic segmentation models for coarse segmentation, followed by refinement processing technologies for overlapping areas (Song *et al.*, 2016; Zhang *et al.*, 2020). These multiple-stage architectures introduce lots of human designs and interventions, leading to increasing training difficulties and poor generalizations. Recently, few studies investigate the feasibility of building end-to-end models by the detect-then-segment paradigm (Zhou *et al.*, 2019a), which detect objects and then segment each detected object in a single learning framework. Although cytological segmentation has made some progress, for complex morphological feature representation, building end-to-end instance segmentation models still remains value to be studied and explored.

5.3. Effective feature representation learning

In deep learning, the performance of downstream tasks will be greatly influenced by the feature representation capability of feature extractors. The main goal of DL models in cytology is to learn effective features of cytology images for cell classification, cellular objects detection and segmentation. Thus, building models that effectively represent features is crucial for cytology image analysis.

Recently, attention mechanism has made promising achievements in effective representation of image features, thus improving performances of down-stream tasks (Vaswani *et al.*, 2017). The deep neural networks with attention modules can reduce the dependence on external information, and be better at capturing internal correlations of data or features. In cytology images, there are too many useless objects, like background, mucus, blood, and inflammatory cells (Hussain *et al.*, 2020a). Attention mechanism-based strategies can make deep models focus more on lesion-related regions or object-related (e.g., nuclei, cytoplasm) regions. Besides, the attention mechanism not only improves the deep learning model but also provides convenience for model visualization and understanding. A few studies have validated the superiority of the attention mechanism in cytology image analysis. Zhang *et al.* (2020) utilized the attention mechanism to enhance U-Net for segmentation of overlapping cervical cells. Besides, Zhou *et al.* (2019a) introduced a multi-head attention mechanism module into the instance segmentation model for improving instance representation. These studies integrated attention modules into the framework and achieved improved performances. After that, the popular structure with attention mechanism, transformer has been demonstrated its superiority of learning global dependencies in various applications (Dosovitskiy *et al.*, 2020). Transformer-based structures are waiting to be investigated in cytology image analysis, such as building dependencies between different cells in patch images, or different regions in WSIs.

5.4. Generalizability and robustness

The generalizability of DL-based algorithms in computational cytology determines whether the model can be success-

fully applied to actual clinical scenarios with various influences. At present, many DL approaches for medical image analysis can obtain acceptable performance in their own datasets, but their clinical performance is far from reaching practical standards (Litjens *et al.*, 2017).

Due to various specimen collection methods, staining techniques and imaging protocols, the data heterogeneity is the key reason for the poor clinical performance. It can lead to the weak robustness and generalization capability of DL models, thus performing poorly when applied to unseen data scenarios. Clinically, the performance of these DL models could degrade significantly, leading to low clinical reproducibility (Kowal *et al.*, 2020).

Extensive researchers are investigating to mitigate this issue. For image processing strategies, normalization methods are utilized to pre-process input data in many image analysis tasks. These methods provide limited benefit in DL-based medical image analysis, because two datasets can be influenced and normalized against each other (Mahmood *et al.*, 2019). For learning strategy, domain adaptation can alleviate this problem by transferring knowledge for decreasing the need for annotations of target tasks (Oza *et al.*, 2021). Domain adaptation has been used for medical scenarios with cross-domain data (e.g., CT and MRI (Chen *et al.*, 2020)), the potential of domain adaptation methods in cytology image analysis remains to be explored. For instance, building cross-domain learning framework to analyze multi-domain images, such as images from multi-center, differently stained cytology images, and even different pathology images (e.g., cytology and histopathology).

Designing new models for robust feature extraction of cytology images is also worthy of being explored, especially for feature extractor, which aims to map cytology images from multi-center to the same feature space for learning domain-invariant representations, thereby addressing the data heterogeneity issue (Li *et al.*, 2021). In addition, multimodal data has been demonstrated to compensate for the missing information in single modality data (Zhang *et al.*, 2021). For medical scenarios, Shao *et al.* (2019) designs a multimodal fusion framework to combine histopathological images and genomic sequences for early-stage cancer prognosis. Similarly, multimodality or full modality learning is also worth exploring and studying in cytology applications.

5.5. Transparency and interpretability

Unlike other deep learning application scenarios, the medical domain not only focuses on the model performance in clinical practice but also its interpretability, which is of paramount importance in clinical decision-making. However, the black-box nature of DL algorithms lacking clinical interpretability and transparency has restricted its clinical adoption (Lu *et al.*, 2021). Therefore, explainable AI for medicine is introduced to establish the confidence between AI technologies and doctors/patients. There are some explorable issues in computational cytology, such as slide-level cytology screening based on rules, and visualization of the decision-making process of deep models.

Visualization is regarded as one of techniques for interpretation. Current techniques mainly utilize attention mechanism

to generate heatmaps to visualize the deep features and models, such as class activation mapping (CAM) (Zhou *et al.*, 2016). In cytology image analysis, a few studies have employed heat maps or feature maps for exploring the decision-making basis of deep learning models in the classification task. Nojima *et al.* (2021) used Grad-CAM to observe the model's high response regions of urothelial cytology images, which can improve medical decision-making from the gradient of the differentiable model. For model-agnostic visualization, another technique, local interpretable model-agnostic explanation (LIME) (Ribeiro *et al.*, 2016) can be effective to provide the interpretability and transparency. LIME presents a locally faithful explanation by fitting a set of perturbed samples near the target sample using a potentially interpretable model. In addition to these mentioned methods, more visualization techniques are under exploration for interpretability.

To increase the credibility of deep models in computational cytology, researchers constructed slide-level screening system by assembling multiple tasks rather than predicting the final diagnosis results of cytology slides, which can assist pathologists to obtain multi-stage analysis results. Zhu *et al.* (2021) integrated DL-based classification, detection, and segmentation models to build a cervical LBC smear TBS diagnostic system. Another study, Lin *et al.* (2021) built a dual-path network for outputting the detected lesions, followed by a rule-based risk stratification system. Wei *et al.* (2021) divided the cervical WSI analysis into two stages, i.e., cervical lesion detection at the patch level in preselected ROIs, and normal/abnormal classification at the WSI level. The output of each stage of these multi-stage methods can provide intermediate explanations for model prediction and cytology screening, thus improving the transparency of the diagnostic process.

5.6. Digital medicine and human-AI collaboration

Digital medicine integrates medicine and information technology for clinical diagnosis and treatment, it aims to transform digital models to clinical scenarios (Beam *et al.*, 2020; Samuel *et al.*, 2020). Although a large number of DL models report that they can achieve state-of-the-art performance, they are mostly validated on domain-specific datasets and cannot achieve the same good performance in clinical practice. Unavailability of data is one of the crucial factors leading to this problem, because data privacy cannot be overemphasized in medicine domain. Currently, privacy-preserving learning approaches are being explored and studied for improving the availability of multi-center data (Chen *et al.*, 2021), e.g., federated learning (Rieke *et al.*, 2020). Another crucial issue facing clinical transformation is that clinical data is usually more diverse and complex than collected training data, caused by variable clinical factors regarding imaging microscopes, staining techniques, patch extraction, and selection, etc. To address this issue, designing more robust architectures can make the model less dependent on data quality in digital medicine. In addition, cytologists analyze specimens of different cancer types using different diagnostic criteria (Nayar and Wilbur, 2015), which makes it difficult for DL algorithms that focus on domain-specific cytology to adapt to different cancer scenarios.

In recent years, numerous studies show that the human-machine collaborative medical diagnosis system can achieve better diagnosis performance than conventional diagnosis systems by the intervention of human experts and assistance of machines (Zhu *et al.*, 2021; Patel *et al.*, 2019). The DL algorithm in the intelligent medical system provides doctors with multi-level, and high-confidence prediction results. Besides, the digital diagnostic system provides doctors with real-time diagnostic information through human-computer interaction technology. The smart microscope system (ARM), designed by Google Health, has made an early breakthrough in this field (Chen *et al.*, 2019). ARM integrates AI algorithms with optical microscope to analyze pathological slides and provide pathologists analysis results (e.g., lesion contour, probability heatmap) in the field of view by augmented reality technologies. Then, pathologists make the final diagnosis based on these quantitative and qualitative results. This computer-assisted diagnostic system has provided prospects for the automation of histopathology, cytology, parasitology, etc. However, there is still a long way to go in terms of accurate and efficient diagnosis, system integration, hardware resources, and AI algorithms.

6. Conclusion

In recent years, the development of deep learning has enabled great success in computational cytology, showing significant promise for efficient cancer screening. In this paper, we have comprehensively reviewed the current progress of deep learning-based methods in computational cytology, including supervised learning, weakly supervised learning, unsupervised learning, and transfer learning. More specifically, we survey image analysis-based approaches and state-of-the-art DL algorithms with the applications of classification, detection, and segmentation in cytology. Various applications of advanced DL-based works of various cytology were investigated in this paper, including the cervix, breast, lung, thyroid, oral, kidney, stomach, etc. We also summarize the evaluation metrics and public datasets for developing new models. Finally, we outline current challenges and potential directions for future research of computational cytology.

Declaration of Competing Interest

The authors declare that they have no known competing financial interests or personal relationships that could have appeared to influence the work reported in this paper.

CRedit authorship contribution statement

Hao Jiang: Conceptualization, Methodology, Writing - original draft, Visualization. **Yanning Zhou:** Conceptualization, Formal analysis, Writing - review & editing. **Yi Lin:** Conceptualization, Writing - review & editing, Investigation. **Ronald CK Chan:** Formal analysis, Writing - review & editing. **Jiang Liu:** Conceptualization, Investigation. **Hao Chen:** Conceptualization, Funding acquisition, Project administration, Resources, Supervision, Writing - review & editing.

Acknowledgments

This work was supported by Beijing Institute of Collaborative Innovation Program (No. BICI22EG01).

References

- Alberts, B., Bray, D., Hopkin, K., Johnson, A.D., Lewis, J., Raff, M., Roberts, K., Walter, P., 2015. *Essential cell biology*. Garland Science.
- Alberts, B., Johnson, A., Lewis, J., Raff, M., Roberts, K., Walter, P., et al., 2003. *Molecular biology of the cell*. Scandinavian Journal of Rheumatology 32, 125–125.
- Albuquerque, T., Cruz, R., Cardoso, J.S., 2021. Ordinal losses for classification of cervical cancer risk. *PeerJ Computer Science* 7, e457.
- Amorim, J.G.A., Macarini, L.A.B., Matias, A.V., Cerentini, A., Onofre, F.B.D.M., Onofre, A.S.C., Von Wangenheim, A., 2020. A novel approach on segmentation of agnored-stained cytology images using deep learning, in: 2020 IEEE 33rd International Symposium on Computer-Based Medical Systems (CBMS), IEEE. pp. 552–557.
- An, Y., Shen, H.W., Shan, G., Li, G., Liu, J., 2021. Stsrnet: Deep joint space-time super-resolution for vector field visualization. *IEEE Computer Graphics and Applications* 41, 122–132.
- Araujo, F.H., Silva, R.R., Ushizima, D.M., Rezende, M.T., Carneiro, C.M., Bianchi, A.G.C., Medeiros, F.N., 2019. Deep learning for cell image segmentation and ranking. *Computerized Medical Imaging and Graphics* 72, 13–21.
- Awan, R., Benes, K., Azam, A., Song, T.H., Shaban, M., Verrill, C., Tsang, Y.W., Snead, D., Minhas, F., Rajpoot, N., 2021. Deep learning based digital cell profiles for risk stratification of urine cytology images. *Cytometry Part A*.
- Bakht, A.B., Javed, S., Dina, R., Almarzouqi, H., Khandoker, A., Werghi, N., 2020. Thyroid nodule cell classification in cytology images using transfer learning approach., in: *International Conference on Soft Computing and Pattern Recognition*, pp. 539–549.
- Bal, A., Das, M., Satapathy, S.M., Jena, M., Das, S.K., 2021. Bfcnet: a cnn for diagnosis of ductal carcinoma in breast from cytology images. *Pattern Analysis and Applications*, 1–14.
- Bao, H., Bi, H., Zhang, X., Zhao, Y., Dong, Y., Luo, X., Zhou, D., You, Z., Wu, Y., Liu, Z., et al., 2020. Artificial intelligence-assisted cytology for detection of cervical intraepithelial neoplasia or invasive cancer: A multicenter, clinical-based, observational study. *Gynecologic Oncology* 159, 171–178.
- Barkan, G.A., Wojcik, E.M., Nayar, R., Savic-Prince, S., Quek, M.L., Kurtycz, D.F., Rosenthal, D.L., 2016. The paris system for reporting urinary cytology: the quest to develop a standardized terminology. *Acta Cytologica* 60, 185–197.
- Baykal, E., Dogan, H., Ercin, M.E., Ersoz, S., Ekinici, M., 2020. Modern convolutional object detectors for nuclei detection on pleural effusion cytology images. *Multimedia Tools and Applications* 79, 15417–15436.
- Beam, A.L., Manrai, A.K., Ghassemi, M., 2020. Challenges to the reproducibility of machine learning models in health care. *Jama* 323, 305–306.
- Beca, F., Schmitt, F.C., 2019. Ancillary tests in breast cytology: a practical guide. *Acta cytologica* 63, 302–313.
- Bhatt, A.R., Ganatra, A., Kotecha, K., 2021. Cervical cancer detection in pap smear whole slide images using convnet with transfer learning and progressive resizing. *PeerJ Computer Science* 7, e348.
- Böhm, A., Tatarchenko, M., Falk, T., 2019. Isoo v2 dl-semantic instance segmentation of touching and overlapping objects, in: 2019 IEEE 16th International Symposium on Biomedical Imaging (ISBI 2019), IEEE. pp. 343–347.
- Brown, A.D., Garber, A.M., 1999. Cost-effectiveness of 3 methods to enhance the sensitivity of papanicolaou testing. *Jama* 281, 347–353.
- Caddy, G., Conron, M., Wright, G., Desmond, P., Hart, D., Chen, R., 2005. The accuracy of eus-fna in assessing mediastinal lymphadenopathy and staging patients with nslc. *European Respiratory Journal* 25, 410–415.
- Çallı, E., Sogancıoğlu, E., van Ginneken, B., van Leeuwen, K.G., Murphy, K., 2021. Deep learning for chest x-ray analysis: A survey. *Medical Image Analysis*, 102125.
- Cao, L., Yang, J., Rong, Z., Li, L., Xia, B., You, C., Lou, G., Jiang, L., Du, C., Meng, H., et al., 2021. A novel attention-guided convolutional network for the detection of abnormal cervical cells in cervical cancer screening. *Medical Image Analysis*, 102197.

- Chai, Z., Luo, L., Lin, H., Chen, H., Heng, P.A., 2021. Deep semi-supervised metric learning with dual alignment for cervical cancer cell detection. arXiv preprint arXiv:2104.03265 .
- Chankong, T., Theera-Umpon, N., Auephanwiriyakul, S., 2014. Automatic cervical cell segmentation and classification in pap smears. *Computer Methods and Programs in Biomedicine* 113, 539–556.
- Chen, C., Dou, Q., Chen, H., Qin, J., Heng, P.A., 2020. Unsupervised bidirectional cross-modality adaptation via deeply synergistic image and feature alignment for medical image segmentation. *IEEE Transactions on Medical Imaging* 39, 2494–2505.
- Chen, H., Dou, Q., Wang, X., Qin, J., Heng, P.A., 2016a. Mitosis detection in breast cancer histology images via deep cascaded networks, in: Thirtieth AAAI conference on artificial intelligence, pp. 1160–1166.
- Chen, H., Qi, X., Yu, L., Dou, Q., Qin, J., Heng, P.A., 2017. Dcan: Deep contour-aware networks for object instance segmentation from histology images. *Medical Image Analysis* 36, 135–146.
- Chen, H., Qi, X., Yu, L., Heng, P.A., 2016b. Dcan: deep contour-aware networks for accurate gland segmentation, in: Proceedings of the IEEE conference on Computer Vision and Pattern Recognition, pp. 2487–2496.
- Chen, M., Zhang, Z., Wang, T., Backes, M., Humbert, M., Zhang, Y., 2021. When machine unlearning jeopardizes privacy, in: Proceedings of the 2021 ACM SIGSAC Conference on Computer and Communications Security, pp. 896–911.
- Chen, P.H.C., Gadepalli, K., MacDonald, R., Liu, Y., Kadowaki, S., Nagpal, K., Kohlberger, T., Dean, J., Corrado, G.S., Hipp, J.D., et al., 2019. An augmented reality microscope with real-time artificial intelligence integration for cancer diagnosis. *Nature Medicine* 25, 1453–1457.
- Cheng, S., Liu, S., Yu, J., Rao, G., Xiao, Y., Han, W., Zhu, W., Lv, X., Li, N., Cai, J., et al., 2021. Robust whole slide image analysis for cervical cancer screening using deep learning. *Nature Communications* 12, 1–10.
- Cibas, E.S., Ali, S.Z., 2017. The 2017 bethesda system for reporting thyroid cytopathology. *Thyroid* 27, 1341–1346.
- Davey, E., Barratt, A., Irwig, L., Chan, S.F., Macaskill, P., Mannes, P., Saville, A.M., 2006. Effect of study design and quality on unsatisfactory rates, cytology classifications, and accuracy in liquid-based versus conventional cervical cytology: a systematic review. *The Lancet* 367, 122–132.
- De Vito, C., Angeloni, C., De Feo, E., Marzuillo, C., Lattanzi, A., Ricciardi, W., Villari, P., Boccia, S., 2014. A large cross-sectional survey investigating the knowledge of cervical cancer risk aetiology and the predictors of the adherence to cervical cancer screening related to mass media campaign. *BioMed Research International* 2014.
- Deng, J., Dong, W., Socher, R., Li, L.J., Li, K., Fei-Fei, L., 2009. Imagenet: A large-scale hierarchical image database, in: 2009 IEEE conference on computer vision and pattern recognition, Ieee, pp. 248–255.
- Dey, P., 2018. Basic and advanced laboratory techniques in histopathology and cytology. Springer.
- Dey, S., Das, S., Ghosh, S., Mitra, S., Chakrabarty, S., Das, N., 2019. Syncgan: Using learnable class specific priors to generate synthetic data for improving classifier performance on cytological images, in: National Conference on Computer Vision, Pattern Recognition, Image Processing, and Graphics, Springer, pp. 32–42.
- Dimauro, G., Ciprandi, G., Deperte, F., Girardi, F., Ladisa, E., Latrofa, S., Gelardi, M., 2019. Nasal cytology with deep learning techniques. *International journal of medical informatics* 122, 13–19.
- Dosovitskiy, A., Beyer, L., Kolesnikov, A., Weissenborn, D., Zhai, X., Unterthiner, T., Dehghani, M., Minderer, M., Heigold, G., Gelly, S., et al., 2020. An image is worth 16x16 words: Transformers for image recognition at scale. arXiv preprint arXiv:2010.11929 .
- Dov, D., Kovalsky, S.Z., Assaad, S., Cohen, J., Range, D.E., Pendse, A.A., Henao, R., Carin, L., 2021. Weakly supervised instance learning for thyroid malignancy prediction from whole slide cytopathology images. *Medical Image Analysis* 67, 101814.
- Dov, D., Kovalsky, S.Z., Cohen, J., Range, D.E., Henao, R., Carin, L., 2019. Thyroid cancer malignancy prediction from whole slide cytopathology images, in: Machine Learning for Healthcare Conference, PMLR, pp. 553–570.
- Elliott Range, D.D., Dov, D., Kovalsky, S.Z., Henao, R., Carin, L., Cohen, J., 2020. Application of a machine learning algorithm to predict malignancy in thyroid cytopathology. *Cancer cytopathology* 128, 287–295.
- Falk, T., Mai, D., Bensch, R., Çiçek, Ö., Abdulkadir, A., Marrakchi, Y., Böhm, A., Deubner, J., Jäckel, Z., Seiwald, K., et al., 2019. U-net: deep learning for cell counting, detection, and morphometry. *Nature Methods* 16, 67–70.
- Field, A.S., Raymond, W.A., Rickard, M., Arnold, L., Brachtel, E.F., Chaiwun, B., Chen, L., Di Bonito, L., Kurtycz, D.F., Lee, A.H., et al., 2019. The international academy of cytology yokohama system for reporting breast fine-needle aspiration biopsy cytopathology. *Acta Cytologica* 63, 257–273.
- Garud, H., Karri, S.P.K., Sheet, D., Chatterjee, J., Mahadevappa, M., Ray, A.K., Ghosh, A., Maity, A.K., 2017. High-magnification multi-views based classification of breast fine needle aspiration cytology cell samples using fusion of decisions from deep convolutional networks, in: Proceedings of the IEEE conference on computer vision and pattern recognition workshops, pp. 76–81.
- Girshick, R., 2015. Fast r-cnn, in: Proceedings of the IEEE international conference on computer vision, pp. 1440–1448.
- Girshick, R., Donahue, J., Darrell, T., Malik, J., 2014. Rich feature hierarchies for accurate object detection and semantic segmentation, in: Proceedings of the IEEE conference on computer vision and pattern recognition, pp. 580–587.
- Gonzalez, D., Dietz, R.L., Pantanowitz, L., 2020. Feasibility of a deep learning algorithm to distinguish large cell neuroendocrine from small cell lung carcinoma in cytology specimens. *Cytopathology* 31, 426–431.
- Goodfellow, I., Pouget-Abadie, J., Mirza, M., Xu, B., Warde-Farley, D., Ozair, S., Courville, A., Bengio, Y., 2014. Generative adversarial nets. *Advances in Neural Information Processing Systems* 27.
- Guan, H., Liu, M., 2021. Domain adaptation for medical image analysis: a survey. arXiv preprint arXiv:2102.09508 .
- Guan, Q., Wan, X., Lu, H., Ping, B., Li, D., Wang, L., Zhu, Y., Wang, Y., Xiang, J., 2019a. Deep convolutional neural network inception-v3 model for differential diagnosing of lymph node in cytological images: a pilot study. *Annals of Translational Medicine* 7.
- Guan, Q., Wang, Y., Ping, B., Li, D., Du, J., Qin, Y., Lu, H., Wan, X., Xiang, J., 2019b. Deep convolutional neural network vgg-16 model for differential diagnosing of papillary thyroid carcinomas in cytological images: a pilot study. *Journal of Cancer* 10, 4876.
- He, K., Gkioxari, G., Dollár, P., Girshick, R., 2017. Mask r-cnn, in: Proceedings of the IEEE international conference on computer vision, pp. 2961–2969.
- He, K., Zhang, X., Ren, S., Sun, J., 2016. Deep residual learning for image recognition, in: Proceedings of the IEEE conference on computer vision and pattern recognition, pp. 770–778.
- Hossain, M.S., Jalab, H.A., Zulfiqar, F., Pervin, M., 2019. Renal cancer cell nuclei detection from cytological images using convolutional neural network for estimating proliferation rate. *Journal of Telecommunication, Electronic and Computer Engineering (JTEC)* 11, 63–71.
- Huang, G., Liu, Z., Van Der Maaten, L., Weinberger, K.Q., 2017. Densely connected convolutional networks, in: Proceedings of the IEEE conference on computer vision and pattern recognition, pp. 4700–4708.
- Hussain, E., Mahanta, L.B., Borah, H., Das, C.R., 2020a. Liquid based-cytology pap smear dataset for automated multi-class diagnosis of precancerous and cervical cancer lesions. *Data in brief* 30, 105589.
- Hussain, E., Mahanta, L.B., Das, C.R., Choudhury, M., Chowdhury, M., 2020b. A shape context fully convolutional neural network for segmentation and classification of cervical nuclei in pap smear images. *Artificial Intelligence in Medicine* 107, 101897.
- Hussain, E., Mahanta, L.B., Das, C.R., Talukdar, R.K., 2020c. A comprehensive study on the multi-class cervical cancer diagnostic prediction on pap smear images using a fusion-based decision from ensemble deep convolutional neural network. *Tissue and Cell* 65, 101347.
- Isa, N.M., 2005. Automated edge detection technique for pap smear images using moving k-means clustering and modified seed based region growing algorithm. *International Journal of The Computer, the Internet and Management* 13, 45–59.
- Ivanovic, M., 2014. Overview of cytopathology procedures and techniques. *Cytopathology in Oncology* , 1–12.
- Jantzen, J., Norup, J., Dounias, G., Bjerregaard, B., 2005. Pap-smear benchmark data for pattern classification. *Nature inspired Smart Information Systems (NiSIS 2005)* , 1–9.
- Ji, A.L., Rubin, A.J., Thrane, K., Jiang, S., Reynolds, D.L., Meyers, R.M., Guo, M.G., George, B.M., Mollbrink, A., Bergensträhle, J., et al., 2020. Multimodal analysis of composition and spatial architecture in human squamous cell carcinoma. *Cell* 182, 497–514.
- Johnston, D., 1952. Cytoplasmic: nuclear ratios in the cytological diagnosis of cancer. *Cancer* 5, 945–949.
- Jónsson, B.A., Björnsdóttir, G., Thorgeirsson, T., Ellingsen, L.M., Walters, G.B., Gudbjartsson, D., Stefansson, H., Stefansson, K., Ulfarsson, M., 2019.

- Brain age prediction using deep learning uncovers associated sequence variants. *Nature Communications* 10, 1–10.
- Kaneko, M., Tsuji, K., Masuda, K., Ueno, K., Henmi, K., Nakagawa, S., Fujita, R., Suzuki, K., Inoue, Y., Teramukai, S., et al., 2021. Urine cell image recognition using a deep learning model for an automated slide evaluation system. *BJU international*.
- Ke, J., Shen, Y., Lu, Y., Deng, J., Wright, J.D., Zhang, Y., Huang, Q., Wang, D., Jing, N., Liang, X., et al., 2021. Quantitative analysis of abnormalities in gynecologic cytopathology with deep learning. *Laboratory Investigation* 101, 513–524.
- Kilic, B., Baykal, E., Ekinci, M., Dogan, H., Ercin, M.E., Ersoz, S., 2019. Automated nuclei detection on pleural effusion cytopathology images using yolov3, in: 2019 4th International Conference on Computer Science and Engineering (UBMK), IEEE. pp. 1–5.
- Kingma, D.P., Welling, M., 2013. Auto-encoding variational bayes. *arXiv preprint arXiv:1312.6114*.
- Kitchener, H.C., Castle, P.E., Cox, J.T., 2006. Achievements and limitations of cervical cytology screening. *Vaccine* 24, S63–S70.
- Kontzoglou, K., Moulakakis, K.G., Konofaos, P., Kyriazi, M., Kyroudes, A., Karakitsos, P., 2005. The role of liquid-based cytology in the investigation of breast lesions using fine-needle aspiration: a cytohistopathological evaluation. *Journal of Surgical Oncology* 89, 75–78.
- Koohbanani, N.A., Jahanifar, M., Tajadin, N.Z., Rajpoot, N., 2020. Nuclick: a deep learning framework for interactive segmentation of microscopic images. *Medical Image Analysis* 65, 101771.
- Koss, L.G., Lin, E., Schreiber, K., Elgert, P., Mango, L., 1994. Evaluation of the papnet™ cytologic screening system for quality control of cervical smears. *American Journal of Clinical Pathology* 101, 220–229.
- Koss, L.G., Melamed, M.R., 2006. Koss' diagnostic cytology and its histopathologic bases, volume 1. Lippincott Williams & Wilkins.
- Kowal, M., Żejmo, M., Skobel, M., Korbicz, J., Monczak, R., 2020. Cell nuclei segmentation in cytological images using convolutional neural network and seeded watershed algorithm. *Journal of Digital Imaging* 33, 231–242.
- Landau, M.S., Pantanowitz, L., 2019. Artificial intelligence in cytopathology: a review of the literature and overview of commercial landscape. *Journal of the American Society of Cytopathology* 8, 230–241.
- Larsen, A.B.L., Sønderby, S.K., Larochelle, H., Winther, O., 2016. Autoencoding beyond pixels using a learned similarity metric, in: International conference on machine learning, PMLR. pp. 1558–1566.
- Lassau, N., Ammari, S., Chouzenoux, E., Gortais, H., Herent, P., Devilder, M., Soliman, S., Meyrignac, O., Talabard, M.P., Lamarque, J.P., et al., 2021. Integrating deep learning ct-scan model, biological and clinical variables to predict severity of covid-19 patients. *Nature Communications* 12, 1–11.
- LeCun, Y., Bottou, L., Bengio, Y., Haffner, P., 1998. Gradient-based learning applied to document recognition. *Proceedings of the IEEE* 86, 2278–2324.
- Lever, J., Trott, P., Webb, A., 1985. Fine needle aspiration cytology. *Journal of Clinical Pathology* 38, 1–11.
- Li, J., Chen, W., Huang, X., Hu, Z., Duan, Q., Li, H., Metaxas, D.N., Zhang, S., 2021. Mixed supervision learning for whole slide image classification. *arXiv preprint arXiv:2107.00934*.
- Li, J., Dou, Q., Yang, H., Liu, J., Fu, L., Zhang, Y., Zheng, L., Zhang, D., 2022. Cervical cell multi-classification algorithm using global context information and attention mechanism. *Tissue and Cell* 74, 101677.
- Li, X., Li, Q., et al., 2019. Detection and classification of cervical exfoliated cells based on faster r-cnn, in: 2019 IEEE 11th international conference on advanced infocomm technology (ICAIT), IEEE. pp. 52–57.
- Liang, Y., Pan, C., Sun, W., Liu, Q., Du, Y., 2021a. Global context-aware cervical cell detection with soft scale anchor matching. *Computer Methods and Programs in Biomedicine* 204, 106061.
- Liang, Y., Tang, Z., Yan, M., Chen, J., Liu, Q., Xiang, Y., 2021b. Comparison detector for cervical cell/clumps detection in the limited data scenario. *Neurocomputing* 437, 195–205.
- Lilli, L., Giarnieri, E., Scardapane, S., 2021. A calibrated multiexit neural network for detecting urothelial cancer cells. *Computational and Mathematical Methods in Medicine* 2021.
- Lin, H., Chen, H., Graham, S., Dou, Q., Rajpoot, N., Heng, P.A., 2019a. Fast scannet: Fast and dense analysis of multi-gigapixel whole-slide images for cancer metastasis detection. *IEEE Transactions on Medical Imaging* 38, 1948–1958.
- Lin, H., Chen, H., Wang, X., Wang, Q., Wang, L., Heng, P.A., 2021. Dual-path network with synergistic grouping loss and evidence driven risk stratification for whole slide cervical image analysis. *Medical Image Analysis* 69, 101955.
- Lin, H., Hu, Y., Chen, S., Yao, J., Zhang, L., 2019b. Fine-grained classification of cervical cells using morphological and appearance based convolutional neural networks. *IEEE Access* 7, 71541–71549.
- Lin, T.Y., Dollár, P., Girshick, R., He, K., Hariharan, B., Belongie, S., 2017a. Feature pyramid networks for object detection, in: Proceedings of the IEEE conference on computer vision and pattern recognition, pp. 2117–2125.
- Lin, T.Y., Goyal, P., Girshick, R., He, K., Dollár, P., 2017b. Focal loss for dense object detection, in: Proceedings of the IEEE international conference on computer vision, pp. 2980–2988.
- Litjens, G., Kooi, T., Bejnordi, B.E., Setio, A.A.A., Ciompi, F., Ghafoorian, M., Van Der Laak, J.A., Van Ginneken, B., Sánchez, C.I., 2017. A survey on deep learning in medical image analysis. *Medical Image Analysis* 42, 60–88.
- Liu, L., Wang, Y., Ma, Q., Tan, L., Wu, Y., Xiao, J., 2020. Artificial classification of cervical squamous lesions in thinprep cytologic tests using a deep convolutional neural network. *Oncology Letters* 20, 1–1.
- Liu, W., Anguelov, D., Erhan, D., Szegedy, C., Reed, S., Fu, C.Y., Berg, A.C., 2016. Ssd: Single shot multibox detector, in: European conference on computer vision, Springer. pp. 21–37.
- Long, J., Shelhamer, E., Darrell, T., 2015. Fully convolutional networks for semantic segmentation, in: Proceedings of the IEEE conference on computer vision and pattern recognition, pp. 3431–3440.
- Lu, M.Y., Williamson, D.F., Chen, T.Y., Chen, R.J., Barbieri, M., Mahmood, F., 2021. Data-efficient and weakly supervised computational pathology on whole-slide images. *Nature Biomedical Engineering* 5, 555–570.
- Lu, Z., Carneiro, G., Bradley, A.P., 2015. An improved joint optimization of multiple level set functions for the segmentation of overlapping cervical cells. *IEEE Transactions on Image Processing* 24, 1261–1272.
- Lu, Z., Carneiro, G., Bradley, A.P., Ushizima, D., Nosrati, M.S., Bianchi, A.G., Carneiro, C.M., Hamarneh, G., 2016. Evaluation of three algorithms for the segmentation of overlapping cervical cells. *IEEE Journal of Biomedical and Health Informatics* 21, 441–450.
- Luo, L., Chen, H., Zhou, Y., Lin, H., Pheng, P.A., 2021. Oxnet: Omni-supervised thoracic disease detection from chest x-rays. *arXiv preprint arXiv:2104.03218*.
- Ma, J., Liu, S., Cheng, S., Chen, R., Liu, X., Chen, L., Zeng, S., 2021. Str-net: Self-texture transfer super-resolution and refocusing network. *IEEE Transactions on Medical Imaging*.
- Ma, J., Yu, J., Liu, S., Chen, L., Li, X., Feng, J., Chen, Z., Zeng, S., Liu, X., Cheng, S., 2020. Pathsgan: Multi-supervised super-resolution for cytopathological images using generative adversarial network. *IEEE Transactions on Medical Imaging* 39, 2920–2930.
- Maharjan, S., Ranabhat, S., Tiwari, M., Bhandari, A., Osti, B.P., Neopane, P., 2017. Exfoliative cytology analysis from different sites of the body. *Journal of Chitwan Medical College* 7, 33–39.
- Mahmood, F., Borders, D., Chen, R.J., McKay, G.N., Salimian, K.J., Baras, A., Durr, N.J., 2019. Deep adversarial training for multi-organ nuclei segmentation in histopathology images. *IEEE Transactions on Medical Imaging* 39, 3257–3267.
- Manna, A., Kundu, R., Kaplun, D., Sinitca, A., Sarkar, R., 2021. A fuzzy rank-based ensemble of cnn models for classification of cervical cytology. *Scientific Reports* 11, 1–18.
- Maron, O., Lozano-Pérez, T., 1998. A framework for multiple-instance learning. *Advances in Neural Information Processing Systems*, 570–576.
- Marzahl, C., Aubreville, M., Bertram, C.A., Stayt, J., Jasensky, A.K., Bartenschlager, F., Fragoso-Garcia, M., Barton, A.K., Elsemann, S., Jabari, S., et al., 2020. Deep learning-based quantification of pulmonary hemosiderophages in cytology slides. *Scientific Reports* 10, 1–10.
- Matias, A.V., Cerentini, A., Macarini, L.A.B., Amorim, J.G.A., Daltoé, F.P., von Wangenheim, A., 2021. Segmentation, detection, and classification of cell nuclei on oral cytology samples stained with papanicolaou. *SN Computer Science* 2, 1–15.
- Mehrotra, R., Mishra, S., Singh, M., Singh, M., 2011. The efficacy of oral brush biopsy with computer-assisted analysis in identifying precancerous and cancerous lesions. *Head & Neck Oncology* 3, 1–8.
- Milletari, F., Navab, N., Ahmadi, S.A., 2016. V-net: Fully convolutional neural networks for volumetric medical image segmentation, in: 2016 fourth international conference on 3D vision (3DV), IEEE. pp. 565–571.
- Miselski, B., Fevens, T., Krzyżak, A., Kowal, M., Monczak, R., 2019. Deep neural networks for breast cancer diagnosis: fine needle biopsy scenario, in: Polish Conference on Biocybernetics and Biomedical Engineering, Springer.

- pp. 131–142.
- Mitra, S., Das, N., Dey, S., Chakraborty, S., Nasipuri, M., Naskar, M.K., 2021. Cytology image analysis techniques toward automation: Systematically revisited. *ACM Computing Surveys (CSUR)* 54, 1–41.
- Mohammed, M.A., Abdurahman, F., Ayalew, Y.A., 2021. Single-cell conventional pap smear image classification using pre-trained deep neural network architectures. *BMC Biomedical Engineering* 3, 11–11.
- Moosavi Tayebi, R., Mu, Y., Dehkharghanian, T., Ross, C., Sur, M., Foley, R., Tizhoosh, H.R., Campbell, C.J., 2021. Histogram of cell types: Deep learning for automated bone marrow cytology. *arXiv e-prints*, arXiv:2107.00000.
- Morrison, W., DeNicola, D., 1993. Advantages and disadvantages of cytology and histopathology for the diagnosis of cancer., in: *Seminars in veterinary medicine and surgery (small animal)*, pp. 222–227.
- Nayar, R., Wilbur, D.C., 2015. *The Bethesda system for reporting cervical cytology: definitions, criteria, and explanatory notes*. Springer.
- Neubeck, A., Van Gool, L., 2006. Efficient non-maximum suppression, in: *18th International Conference on Pattern Recognition (ICPR '06)*, IEEE. pp. 850–855.
- Nojima, S., Terayama, K., Shimoura, S., Hijiki, S., Nonomura, N., Morii, E., Okuno, Y., Fujita, K., 2021. A deep learning system to diagnose the malignant potential of urothelial carcinoma cells in cytology specimens. *Cancer Cytopathology*.
- Noyan, M.A., Durdu, M., Eskiocak, A.H., 2020. Tzancknet: a convolutional neural network to identify cells in the cytology of erosive-vesiculobullous diseases. *Scientific Reports* 10, 1–7.
- Oza, P., Sindagi, V.A., VS, V., Patel, V.M., 2021. Unsupervised domain adaptation of object detectors: A survey. *arXiv preprint arXiv:2105.13502*.
- O'Flynn, H., Ryan, N.A., Narine, N., Shelton, D., Rana, D., Crosbie, E.J., 2021. Diagnostic accuracy of cytology for the detection of endometrial cancer in urine and vaginal samples. *Nature Communications* 12, 1–8.
- Patel, B.N., Rosenberg, L., Willcox, G., Baltaxe, D., Lyons, M., Irvin, J., Rajpurkar, P., Amrhein, T., Gupta, R., Halabi, S., et al., 2019. Human-machine partnership with artificial intelligence for chest radiograph diagnosis. *NPJ Digital Medicine* 2, 1–10.
- Phoulady, H.A., Mouton, P.R., 2018. A new cervical cytology dataset for nucleus detection and image classification (cervix93) and methods for cervical nucleus detection. *arXiv preprint arXiv:1811.09651*.
- Pirovano, A., Almeida, L.G., Ladjal, S., Bloch, I., Berlemont, S., 2021. Computer-aided diagnosis tool for cervical cancer screening with weakly supervised localization and detection of abnormalities using adaptable and explainable classifier. *Medical Image Analysis*, 102167.
- Plissiti, M., Tripoliti, E., Charchanti, A., Krikoni, O., Fotiadis, D., 2009. Automated detection of cell nuclei in pap stained cervical smear images using fuzzy clustering, in: *4th European Conference of the International Federation for Medical and Biological Engineering*, Springer. pp. 637–641.
- Plissiti, M.E., Dimitrakopoulos, P., Sfikas, G., Nikou, C., Krikoni, O., Charchanti, A., 2018. Sipakmed: A new dataset for feature and image based classification of normal and pathological cervical cells in pap smear images, in: *2018 25th IEEE International Conference on Image Processing (ICIP)*, IEEE. pp. 3144–3148.
- Rahaman, M.M., Li, C., Wu, X., Yao, Y., Hu, Z., Jiang, T., Li, X., Qi, S., 2020. A survey for cervical cytopathology image analysis using deep learning. *IEEE Access* 8, 61687–61710.
- Rahaman, M.M., Li, C., Yao, Y., Kulwa, F., Wu, X., Li, X., Wang, Q., 2021. Deepcervix: A deep learning-based framework for the classification of cervical cells using hybrid deep feature fusion techniques. *arXiv preprint arXiv:2102.12191*.
- kour Raina, M., Gupta, N., Kumar, S., Kusum, A., 2021. Evaluation of cell block technique versus conventional cytology on bronchoscopy guided needle aspiration/brush cytology for diagnosis of lung cancer. *International Journal of Scientific Research* 10.
- Redmon, J., Divvala, S., Girshick, R., Farhadi, A., 2016. You only look once: Unified, real-time object detection, in: *Proceedings of the IEEE conference on computer vision and pattern recognition*, pp. 779–788.
- Ren, S., He, K., Girshick, R., Sun, J., 2015. Faster r-cnn: Towards real-time object detection with region proposal networks. *Advances in Neural Information Processing Systems* 28, 91–99.
- Rezatofghi, H., Tsoi, N., Gwak, J., Sadeghian, A., Reid, I., Savarese, S., 2019. Generalized intersection over union: A metric and a loss for bounding box regression, in: *Proceedings of the IEEE/CVF Conference on Computer Vision and Pattern Recognition*, pp. 658–666.
- Rezende, M.T., Silva, R., Bernardo, F.d.O., Tobias, A.H., Oliveira, P.H., Machado, T.M., Costa, C.S., Medeiros, F.N., Ushizima, D.M., Carneiro, C.M., et al., 2021. Cric searchable image database as a public platform for conventional pap smear cytology data. *Scientific Data* 8, 1–8.
- Ribeiro, M.T., Singh, S., Guestrin, C., 2016. "why should i trust you?" explaining the predictions of any classifier, in: *Proceedings of the 22nd ACM SIGKDD international conference on knowledge discovery and data mining*, pp. 1135–1144.
- Rieke, N., Hancox, J., Li, W., Milletari, F., Roth, H.R., Albarqouni, S., Bakas, S., Galtier, M.N., Landman, B.A., Maier-Hein, K., et al., 2020. The future of digital health with federated learning. *NPJ Digital Medicine* 3, 1–7.
- Ronneberger, O., Fischer, P., Brox, T., 2015. U-net: Convolutional networks for biomedical image segmentation, in: *International Conference on Medical image computing and computer-assisted intervention*, Springer. pp. 234–241.
- Rosenblatt, F., 1961. *Principles of neurodynamics. perceptrons and the theory of brain mechanisms*. Technical Report. Cornell Aeronautical Lab Inc Buffalo NY.
- Rosenthal, D.L., Wojcik, E.M., Kurtycz, D.F., 2016. *The Paris system for reporting urinary cytology*. Springer.
- Rosenzweig, J., Bartl, M., 2015. A review and analysis of literature on autonomous driving. *E-Journal Making-of Innovation*, 1–57.
- Rumelhart, D.E., Hinton, G.E., Williams, R.J., 1986. Learning representations by back-propagating errors. *Nature* 323, 533–536.
- Russell, B.C., Torralba, A., Murphy, K.P., Freeman, W.T., 2008. Labelme: a database and web-based tool for image annotation. *International Journal of Computer Vision* 77, 157–173.
- Saikia, A.R., Bora, K., Mahanta, L.B., Das, A.K., 2019. Comparative assessment of cnn architectures for classification of breast fnac images. *Tissue and Cell* 57, 8–14.
- Samuel, S., Löffler, F., König-Ries, B., 2020. Machine learning pipelines: provenance, reproducibility and fair data principles. *arXiv preprint arXiv:2006.12117*.
- Van de Sande, K.E., Uijlings, J.R., Gevers, T., Smeulders, A.W., 2011. Segmentation as selective search for object recognition, in: *2011 international conference on computer vision*, IEEE. pp. 1879–1886.
- Sanyal, P., Mukherjee, T., Barui, S., Das, A., Gangopadhyay, P., 2018. Artificial intelligence in cytopathology: a neural network to identify papillary carcinoma on thyroid fine-needle aspiration cytology smears. *Journal of pathology informatics* 9.
- Selvaraju, R.R., Cogswell, M., Das, A., Vedantam, R., Parikh, D., Batra, D., 2017. Grad-cam: Visual explanations from deep networks via gradient-based localization, in: *Proceedings of the IEEE international conference on computer vision*, pp. 618–626.
- Shanthi, P., Faruqi, F., Hareesha, K., Kudva, R., 2019. Deep convolution neural network for malignancy detection and classification in microscopic uterine cervix cell images. *Asian Pacific Journal of Cancer Prevention: APJCP* 20, 3447.
- Shao, W., Han, Z., Cheng, J., Cheng, L., Wang, T., Sun, L., Lu, Z., Zhang, J., Zhang, D., Huang, K., 2019. Integrative analysis of pathological images and multi-dimensional genomic data for early-stage cancer prognosis. *IEEE Transactions on Medical Imaging* 39, 99–110.
- Shi, J., Wang, R., Zheng, Y., Jiang, Z., Zhang, H., Yu, L., 2021. Cervical cell classification with graph convolutional network. *Computer Methods and Programs in Biomedicine* 198, 105807.
- Skaarland, E., 1986. New concept in diagnostic endometrial cytology: diagnostic criteria based on composition and architecture of large tissue fragments in smears. *Journal of Clinical Pathology* 39, 36–43.
- Sompawong, N., Mopan, J., Pooprasert, P., Himakhun, W., Suwannaruk, K., Ngamvirojcharoen, J., Vachiramon, T., Tantibundhit, C., 2019. Automated pap smear cervical cancer screening using deep learning, in: *2019 41st Annual International Conference of the IEEE Engineering in Medicine and Biology Society (EMBC)*, IEEE. pp. 7044–7048.
- Song, Y., Tan, E.L., Jiang, X., Cheng, J.Z., Ni, D., Chen, S., Lei, B., Wang, T., 2016. Accurate cervical cell segmentation from overlapping clumps in pap smear images. *IEEE transactions on medical imaging* 36, 288–300.
- Song, Y., Zhang, L., Chen, S., Ni, D., Lei, B., Wang, T., 2015. Accurate segmentation of cervical cytoplasm and nuclei based on multiscale convolutional network and graph partitioning. *IEEE Transactions on Biomedical Engineering* 62, 2421–2433.
- Song, Y., Zhang, L., Chen, S., Ni, D., Li, B., Zhou, Y., Lei, B., Wang, T., 2014. A deep learning based framework for accurate segmentation of cervical cytoplasm and nuclei, in: *2014 36th Annual International Conference of the*

- IEEE Engineering in Medicine and Biology Society, IEEE. pp. 2903–2906.
- Song, Y., Zhu, L., Lei, B., Sheng, B., Dou, Q., Qin, J., Choi, K.S., 2020. Shape mask generator: Learning to refine shape priors for segmenting overlapping cervical cytoplasm, in: *International Conference on Medical Image Computing and Computer-Assisted Intervention*, Springer. pp. 639–649.
- Sornapudi, S., Brown, G.T., Xue, Z., Long, R., Allen, L., Antani, S., 2019. Comparing deep learning models for multi-cell classification in liquid-based cervical cytology image, in: *AMIA Annual Symposium Proceedings*, American Medical Informatics Association. p. 820.
- Srinidhi, C.L., Ciga, O., Martel, A.L., 2020. Deep neural network models for computational histopathology: A survey. *Medical Image Analysis*, 101813.
- Su, F., Sun, Y., Hu, Y., Yuan, P., Wang, X., Wang, Q., Li, J., Ji, J.F., 2020. Development and validation of a deep learning system for ascites cytopathology interpretation. *Gastric Cancer* 23, 1041–1050.
- Sundararajan, M., Taly, A., Yan, Q., 2017. Axiomatic attribution for deep networks, in: *International Conference on Machine Learning*, PMLR. pp. 3319–3328.
- Szegedy, C., Liu, W., Jia, Y., Sermanet, P., Reed, S., Anguelov, D., Erhan, D., Vanhoucke, V., Rabinovich, A., 2015. Going deeper with convolutions, in: *Proceedings of the IEEE conference on computer vision and pattern recognition*, pp. 1–9.
- Tan, X., Li, K., Zhang, J., Wang, W., Wu, B., Wu, J., Li, X., Huang, X., 2021. Automatic model for cervical cancer screening based on convolutional neural network: a retrospective, multicohort, multicenter study. *Cancer Cell International* 21, 1–10.
- Tareef, A., Song, Y., Huang, H., Wang, Y., Feng, D., Chen, M., Cai, W., 2017. Optimizing the cervix cytological examination based on deep learning and dynamic shape modeling. *Neurocomputing* 248, 28–40.
- Tay, Y., Dehghani, M., Bahri, D., Metzler, D., 2020. Efficient transformers: A survey. *arXiv preprint arXiv:2009.06732*.
- Teramoto, A., Tsukamoto, T., Kiriya, Y., Fujita, H., 2017. Automated classification of lung cancer types from cytological images using deep convolutional neural networks. *BioMed research international* 2017.
- Teramoto, A., Tsukamoto, T., Yamada, A., Kiriya, Y., Imaizumi, K., Saito, K., Fujita, H., 2020. Deep learning approach to classification of lung cytological images: Two-step training using actual and synthesized images by progressive growing of generative adversarial networks. *PloS one* 15, e0229951.
- Teramoto, A., Yamada, A., Kiriya, Y., Tsukamoto, T., Yan, K., Zhang, L., Imaizumi, K., Saito, K., Fujita, H., 2019. Automated classification of benign and malignant cells from lung cytological images using deep convolutional neural network. *Informatics in Medicine Unlocked* 16, 100205.
- Teramoto, A., Yamada, A., Tsukamoto, T., Kiriya, Y., Sakurai, E., Shioyama, K., Michiba, A., Imaizumi, K., Saito, K., Fujita, H., 2021. Mutual stain conversion between giemsa and papanicolaou in cytological images using cycle generative adversarial network. *Heliyon* 7, e06331.
- Tian, Z., Shen, C., Chen, H., He, T., 2019. Fcos: Fully convolutional one-stage object detection, in: *Proceedings of the IEEE/CVF international conference on computer vision*, pp. 9627–9636.
- Tolles, W.E., 1955. Section of biology: The cytoanalyzer—an example of physics in medical research. *Transactions of the New York Academy of Sciences* 17, 250–256.
- Tolles, W.E., Bostrom, R., 1956. Automatic screening of cytological smears for cancer: the instrumentation. *Annals of the New York Academy of Sciences* 63, 1211–1218.
- Tomczak, K., Czerwińska, P., Wizerowicz, M., 2015. The cancer genome atlas (tcga): an immeasurable source of knowledge. *Contemporary Oncology* 19, A68.
- Vaickus, L.J., Suriawinata, A.A., Wei, J.W., Liu, X., 2019. Automating the paris system for urine cytopathology—a hybrid deep-learning and morphometric approach. *Cancer Cytopathology* 127, 98–115.
- Vaswani, A., Shazeer, N., Parmar, N., Uszkoreit, J., Jones, L., Gomez, A.N., Kaiser, L., Polosukhin, I., 2017. Attention is all you need, in: *Advances in neural information processing systems*, pp. 5998–6008.
- Walter, F.C., Damrich, S., Hamprecht, F.A., 2021. Multistar: Instance segmentation of overlapping objects with star-convex polygons, in: *2021 IEEE 18th International Symposium on Biomedical Imaging (ISBI)*, IEEE. pp. 295–298.
- Wan, T., Xu, S., Sang, C., Jin, Y., Qin, Z., 2019. Accurate segmentation of overlapping cells in cervical cytology with deep convolutional neural networks. *Neurocomputing* 365, 157–170.
- Wang, M., Deng, W., 2021. Deep face recognition: A survey. *Neurocomputing* 429, 215–244.
- Wei, Z., Cheng, S., Liu, X., Zeng, S., 2021. An efficient cervical whole slide image analysis framework based on multi-scale semantic and spatial deep features. *arXiv preprint arXiv:2106.15113*.
- Wilbur, D.C., Black-Schaffer, W.S., Luff, R.D., Abraham, K.P., Kemper, C., Molina, J.T., Tench, W.D., 2009. The becton dickinson focalpoint gs imaging system: clinical trials demonstrate significantly improved sensitivity for the detection of important cervical lesions. *American Journal of Clinical Pathology* 132, 767–775.
- Wu, M., Yan, C., Liu, H., Liu, Q., Yin, Y., 2018. Automatic classification of cervical cancer from cytological images by using convolutional neural network. *Bioscience reports* 38, BSR20181769.
- Xiang, Y., Sun, W., Pan, C., Yan, M., Yin, Z., Liang, Y., 2020. A novel automation-assisted cervical cancer reading method based on convolutional neural network. *Biocybernetics and Biomedical Engineering* 40, 611–623.
- Xie, Y., Xing, F., Shi, X., Kong, X., Su, H., Yang, L., 2018. Efficient and robust cell detection: A structured regression approach. *Medical Image Analysis* 44, 245–254.
- Xu, Y., Mo, T., Feng, Q., Zhong, P., Lai, M., Eric, I., Chang, C., 2014. Deep learning of feature representation with multiple instance learning for medical image analysis, in: *2014 IEEE international conference on acoustics, speech and signal processing (ICASSP)*, IEEE. pp. 1626–1630.
- Yi, X., Walia, E., Babyn, P., 2019. Generative adversarial network in medical imaging: A review. *Medical Image Analysis* 58, 101552.
- Yosinski, J., Clune, J., Bengio, Y., Lipson, H., 2014. How transferable are features in deep neural networks? *arXiv preprint arXiv:1411.1792*.
- Yu, J., Jiang, Y., Wang, Z., Cao, Z., Huang, T., 2016. Unitbox: An advanced object detection network, in: *Proceedings of the 24th ACM international conference on Multimedia*, pp. 516–520.
- Yu, S., Zhang, S., Wang, B., Dun, H., Xu, L., Huang, X., Shi, E., Feng, X., 2021. Generative adversarial network based data augmentation to improve cervical cell classification model. *Mathematical Biosciences and Engineering: MBE* 18, 1740–1752.
- Zaremba, W., Sutskever, I., Vinyals, O., 2014. Recurrent neural network regularization. *arXiv preprint arXiv:1409.2329*.
- Żejmo, M., Kowal, M., Korbicz, J., Monczak, R., 2017. Classification of breast cancer cytological specimen using convolutional neural network, in: *Journal of Physics: Conference Series*, IOP Publishing. p. 012060.
- Zhang, C., Liu, D., Wang, L., Li, Y., Chen, X., Luo, R., Che, S., Liang, H., Li, Y., Liu, S., et al., 2019. Dccl: a benchmark for cervical cytology analysis, in: *International Workshop on Machine Learning in Medical Imaging*, Springer. pp. 63–72.
- Zhang, H., Zhu, H., Ling, X., 2020. Polar coordinate sampling-based segmentation of overlapping cervical cells using attention u-net and random walk. *Neurocomputing* 383, 212–223.
- Zhang, L., Kong, H., Ting Chin, C., Liu, S., Fan, X., Wang, T., Chen, S., 2014. Automation-assisted cervical cancer screening in manual liquid-based cytology with hematoxylin and eosin staining. *Cytometry Part A* 85, 214–230.
- Zhang, L., Lu, L., Nogues, I., Summers, R.M., Liu, S., Yao, J., 2017. Deeppap: deep convolutional networks for cervical cell classification. *IEEE journal of biomedical and health informatics* 21, 1633–1643.
- Zhang, Y., Sidibé, D., Morel, O., Mériaudeau, F., 2021. Deep multimodal fusion for semantic image segmentation: A survey. *Image and Vision Computing* 105, 104042.
- Zhao, Z., Lin, H., Chen, H., Heng, P.A., 2019. Pfa-scanner: Pyramidal feature aggregation with synergistic learning for breast cancer metastasis analysis, in: *International Conference on Medical Image Computing and Computer-Assisted Intervention*, Springer. pp. 586–594.
- Zheng, Z., Wang, P., Liu, W., Li, J., Ye, R., Ren, D., 2020. Distance-iou loss: Faster and better learning for bounding box regression, in: *Proceedings of the AAAI Conference on Artificial Intelligence*, pp. 12993–13000.
- Zhou, B., Khosla, A., Lapedriza, A., Oliva, A., Torralba, A., 2016. Learning deep features for discriminative localization, in: *Proceedings of the IEEE conference on computer vision and pattern recognition*, pp. 2921–2929.
- Zhou, Y., Chen, H., Lin, H., Heng, P.A., 2020. Deep semi-supervised knowledge distillation for overlapping cervical cell instance segmentation, in: *International Conference on Medical Image Computing and Computer-Assisted Intervention*, Springer. pp. 521–531.
- Zhou, Y., Chen, H., Xu, J., Dou, Q., Heng, P.A., 2019a. Inet: Instance relation network for overlapping cervical cell segmentation, in: *International Conference on Medical Image Computing and Computer-Assisted Intervention*,

- Springer. pp. 640–648.
- Zhou, Y., Onder, O.F., Dou, Q., Tsougenis, E., Chen, H., Heng, P.A., 2019b. Cia-net: Robust nuclei instance segmentation with contour-aware information aggregation, in: International Conference on Information Processing in Medical Imaging, Springer. pp. 682–693.
- Zhou, Z.H., 2018. A brief introduction to weakly supervised learning. *National Science Review* 5, 44–53.
- Zhu, J.Y., Park, T., Isola, P., Efros, A.A., 2017. Unpaired image-to-image translation using cycle-consistent adversarial networks, in: Proceedings of the IEEE international conference on computer vision, pp. 2223–2232.
- Zhu, X., Li, X., Ong, K., Zhang, W., Li, W., Li, L., Young, D., Su, Y., Shang, B., Peng, L., et al., 2021. Hybrid ai-assistive diagnostic model permits rapid tbs classification of cervical liquid-based thin-layer cell smears. *Nature Communications* 12, 1–12.